ASSESSMENT OF SUBCOOLED CHOKING FLOW MODELS IN RELAP5 WITH EXPERIMENTAL DATA IN SIMULATED STEAM GENERATOR TUBE CRACKS

by

Mark A. Brown

A Thesis

Submitted to the Faculty of Purdue University

In Partial Fulfillment of the Requirements for the degree of

Master of Science in Nuclear Engineering

School of Nuclear Engineering

West Lafayette, Indiana

December 2018

THE PURDUE UNIVERSITY GRADUATE SCHOOL
STATEMENT OF COMMITTEE APPROVAL

Dr. Shripad T. Revankar, Chair

School of Nuclear Engineering

Dr. Rusi Taleyarkhan

School of Nuclear Engineering

Dr. Jovica R. Riznic

Technical Specialist at the Operational Engineering Assessment Division of the Canadian Nuclear Safety Commission

Approved by:

Dr. Seungjin Kim

Head of the Graduate Program

To my loving parents and family

ACKNOWLEDGMENTS

I would like to take this opportunity to express my deep gratitude to Professor Shripad T. Revankar for his support, guidance, and encouragement during my study. I am also grateful to Dr Rusi P. Taleyarkhan and Dr. Jovica R. Riznic for their attendance on my committee. Finally, I would like to thank my dear friends Dr. Tom Adams, Darrell Cheu, Andrew Fairbanks, and Hung Nguyen for their support, help, and friendship.

TABLE OF CONTENTS

LIST OF TABLES

LIST OF FIGURES

NOMENCLATURE

a	area of a pixel [mm^2]
	sound speed [m/s]
A	*crack's* area [m^2]
C_d	discharge coefficient
C_p	specific heat [$\frac{J}{kg-K}$]
D	*hydraulic* diameter [m]
f	friction factor
g	acceleration of gravity [$\frac{m}{s^2}$]
g_c	Newton constant [$\frac{m^3}{kg-s^2}$]
G	mass flux [kg/m^2s]
h	specific enthalpy [$\frac{J}{kg}$]
h_{fg}	latent heat of vaporization [$\frac{J}{kg}$]
k	conductivity [$W/m^2 \cdot C$]
l	length of a pixel [mm]
L	crack length [m]
	crack's channel length [m]
m	mass flow rate [kg/s]
m_{cond}	condensed mass [kg]
M	number of pixels inside a crack
N	number of pixels in 1mm length
experimental non-equilibrium parameter	
p	crack's wetted parameter [mm]
P	pressure [Pa]
q''	heat flux [W/m^2]
Q	heat Transfer Rate [W]

R	radius [m]
Re	Reynolds number
s	entropy [$\frac{\text{J}}{\text{kg-K}}$]
s_{fg}	entropy of vaporization [$\frac{\text{J}}{\text{kg-K}}$]
S	pressure undershoot correction factor
	slip ratio
t	time [s]
T	temperature [C]
u	fluid velocity [m/s]
x	flow quality
z	channel length variable [m]
Z	number of pixels along perimeter of a crack

Greek Symbols

α	linear expansion coefficient [1/C]
γ	isentropic exponent
η	polytropic exponent
μ	dynamic viscosity [kg/m·s]
υ	specific volume [m^3/kg]
v_f	saturated liquid specific volume [m^3/kg]
v_g	vapor or gas specific volume [m^3/kg]
v_l	liquid specific volume [m^3/kg]
υ_{fg}	υg- υf [m^3/kg]
ρ	density [kg/m^3]
Σ	rate of depressurization [kg/m-s3]
σ	surface tension [kg/s^2]

Subscripts

0	initial condition of a crack before the experiment
	stagnation condition
a	speed of sound
b	back pressure
c	critical (choking) flow
d	pressure undershoot
e	entrance
eq	equilibrium
ex	exit
exp	experimental data point
eq	equilibrium
f	saturated liquid phase
fl	flashing
g	vapor or gas phase
HE	homogeneous equilibrium
l	liquid
s	constant entropy
sat	saturation
t	throat
T	constant temperature

Acronyms

LC	Load Cell
DP	Differential Pressure Transducer
HNEM	Homogeneous Non-Equilibrium Model
H-F	Henry-Fauske
R-T	Ransom-Trapp
CANDU	Canadian Natural Uranium Deuterium
LWR	Light Water Reactor
ODSCC	Outside Diameter Stress Corrosion Cracking

PWR	Pressurized Water Reactor
PWSCC	Pressurized Water Stress Corrosion Cracks

ABSTRACT

Author: Brown, Mark A. MSNE
Institution: Purdue University
Degree Received: December 2018
Title: Assessment of Subcooled Choking Flow Models in RELAP5 with Experimental Data in Simulated Steam Generator Tube Cracks
Committee Chair: Shripad T. Revankar

Choking flow plays an integral part not only in the engineered safeguards of a nuclear power plant (NPP), but also to everyday operation. Current pressurized water reactor steam generators operate on the leak-before-break approach. The ability to predict and estimate a leak rate through a steam generator tube crack is an important safety parameter. Knowledge of the maximum flow rate through a crack in the steam generator tube allows the coolant inventory to be monitored accordingly. Here an assessment of the choking flow models in thermal-hydraulics code RELAP5/MOD3.3 is performed and its suitability to predict choking flow rates through small simulated cracks of steam generator tubes is evaluated based on collected experimental data. Six samples of the data were studied in this work which correspond to steam generator tube crack samples 6-11. Each sample has a wall thickness, channel length (L), of 1.14 mm. Exit areas of these samples, 6-11, are 2.280E-06 m^2, 2.277E-06 m^2, 2.493E-06 m^2, 1.997E-06 m^2, 1.337E-06 m^2, and 2.492E-06 m^2. Samples 6-11 have a channel length to hydraulics diameter ratio (L/D) between 3.0-5.3. Two separate pressure differentials of 6.89 MPa and 4.13 MPa were applied across the samples with a range of subcooling from 20℃ to 80℃ and 20℃ to 60℃. Flow rates through these samples were modeled using the thermal-hydraulic system code RELAP5/MOD3.3. Simulation results are compared to experimental values and modeling techniques are discussed. It is found that both the Henry-Fauske and Ransom-Trapp models better predict choking mass flux for longer channels.

1. INTRODUCTION

In the United States, nuclear power plants have been in commercial use since the late 1950's. According to the U.S. Energy Information Administration, there are sixty NPP in thirty states with ninety-eight operating reactors, which provides 20% of the nation's electrical use. Of these ninety-eight reactors, sixty-five are PWR. Major component problems on the secondary side of PWR's still remain. Commercial steam generator (SG) tubes have experienced degradation and in-service corrosion. This has attracted the interest of this research since these tubes are operating on the leak before break approach.

When water at high temperature and pressure is suddenly depressurized, it passes from a subcooled liquid state to a superheated state. The minimum depressurization pressure will be met and at this point the fluid will flash. In the case of a loss of coolant accident (LOCA) or a leak of through wall steam generator (SG) tube cracks, this discharge depends upon the geometry of the break, upstream pressure conditions, and thermodynamic properties. Moreover, the concern in a NPP is having a metastable fluid leaking at the point of critical flow. This metastability has been well studied for long tubes with large L/D and is challenging to predict [1], [2], [3], [4], [5], [6], [7]

The current experimental study is focused on small narrow crack geometries, where the subcooled liquid flashes into two phase flow under thermal non-equilibrium conditions. In this case, the rate of depressurization can be greater than the thermal exchange rate between two phases which makes the liquid superheated [10]. It is expected more liquid will leak out over a short channel than current models predict do to an increase in the depressurization rate and delay in the development of the two-phase mixture.

The choking flow models currently being explored are based on the homogeneous equilibrium model (HEM) and the homogeneous non-equilibrium model (HNEM). The HEM neglects the slip between liquid and vapor phase, while each phase is in thermal equilibrium. This allows saturation properties of the liquid to be used in the calculation by assuming the fluid to be in thermal and mechanical equilibrium. The point of flashing is a great concern as the subcooled fluid may flash at the entrance or exit of the channel. The HNEM implements a delay time for nucleation and accounts for thermal non-equilibrium due to the nucleation at the choking plane. There are many phenomena influencing the two-phase flow formation and a model which

accurately represents the physics occurring needs to be explored [11]. This study will assess the current available models of best estimate code RELAP5/MOD3.3; however, these models were developed for long channels. This study will focus on short channels (1.14 mm) and the reliability of the code models.

1.1 Objective

The scope of the project was to record the experimental data and assess current subcooled choking flow models in RELAP5/MOD3.3 for simulated steam generator tube cracks. This will allow the Canadian Nuclear Safety Commission (CNSC) to build upon the current database of previous fabricated samples. Unique to this experiment, the samples were fabricated with a very short channel length and smooth surface roughness.

The following objectives were defined for the research project.

i. To develop experimental program which includes:
    a. Improvement of the design of the experimental test facility
    b. The design and manufacturing of simulated steam generator crack test specimens with small increasing fixed channel length (1.14 mm) to hydraulic diameter ratios
    c. Experiments at a maximum pressure of 6.89 MPa
ii. To assess RELAP5 code models for predicting choking flow mass flux

There have been many studies both theoretical and experimental on choking flow. Very few studies however have the same geometric setup. Some focus on slits, some large pipe breaks, and some converging or diverging nozzles. It is therefore difficult to translate these results to the specific problem of steam generator tube cracks. It is theorized that with such small length to diameter ratio in steam generator tube cracks, the non-equilibrium effects will play a significant role in the flow. There will be a very large pressure gradient at the choking plane and there will not be a sufficient amount of time for thermal equilibrium to take place.

1.2 Steam Generator Tube Degradation

Current operational recirculating steam generators for PWR’s worldwide are highly

susceptible to corrosion and mechanical damage. The degradation mechanisms of the SG tubes often require unexpected and extended outages for regulated safety integrity inspections. Though these problems exist not only on the primary side but also on the secondary side, the majority were reported within the United States to have occurred on the secondary side. Efforts have been made to improve designs, materials, and water chemistry; however, these mechanisms are only able to be minimized and continue to be a challenge for the industry [12]. A comprehensive review of the potential degradation mechanisms is listed below. The definitions are adapted from the IAEA and EPRI [12], [13].

- *Outer Diameter Stress Corrosion Cracking (ODSCC)*

  Outer-diameter stress corrosion cracking includes both intergranular stress corrosion cracking (IGSCC) and intergranular attack (IGA) on the outer surface of the tubing. These mechanisms are associated with tensile stresses, impurity concentrations, and sensitivity of materials. The problematic failure modes consist of axial cracks along the tube to tube sheet crevices, tube support plate, and the free span between supports.

- *Primary Water Stress Corrosion Cracking (PWSCC)*

  Primary water stress corrosion cracking occurs on the inside surface of the tubes where there is an absence of intergranular carbides. PWSCC is a thermally activated process and obviously predominantly observed on the hot leg side of recirculating steam generators. A small decrease in the operating temperature significantly slows the initiation and growth of PWSCC. This can be described by the Arrhenius relationship. Axial cracks developed through PWSCC will experience leaks before critical crack size is achieved. This results in the tubes being plugged or sleeved to avoid possible tube rupture.

- *Denting*

  Denting is a mechanical deformation or constriction of a tube near the support plates. This is typically caused by the build-up of deposits (i.e. magnetite) within the annulus of the tube and support plates. Denting in turn affects the flow in the tube and can lead to a decrease in the fatigue resistance as well as heat transfer characteristics.

- *High Cyclic Fatigue*

  The combination of high vibrations and low fatigue strength can result in failure. The flow induced vibrations near the U-Bend region are accompanied with residual stresses. Tubes which have an initiated defect (dent, crack, pit, etc.) are susceptible to high cyclic fatigue.

- *Tube Wear and Fretting*

  Wear and fretting cause axial cracks when tubes come into contact. The small amplitude friction of the contacting surfaces induces the wear of the tube. These mechanisms are a result of flow induced vibrations due to cross flow or local turbulence.

Any of the above listed mechanism may cause a SG tube defect; however, they will not directly lead to leak-before-break (LBB) analyses. These mechanisms over time will need to develop into through wall cracks in order to obtain leak rate behavior focused within this study. In 1993, approximately 68% of all plugged tubes were due to PWSCC, ODSCC, and fretting [13]. As a result of the degrading SG tubes, utilities are faced with high operation and maintenance costs or deration of the plant. Subsequently, if these problems aren't sufficiently maintained, a replacement of the SG is considered to ensure the overall safety of the NPP [14].

1.3 Choking Flow in Literature

The phenomena of two-phase critical flow limit the discharge rates in a LOCA scenario; however, efforts to analyze mechanical and thermal non-equilibrium effects are complicated. The phase change from liquid to two-phase mixture can be separated into stages. Initially subcooled liquid undergoes a pressure drop and reaches saturation. A further reduction in pressure requires the fluid to become superheated and nucleation to occur. This is due to the pressure dropping well below the saturation point of the fluid, thus a departure of thermal equilibrium between phases. This will serve as a starting point for rapid vapor generation or what is known as flashing [15], [16]. It is important to gain quantitative insight of these non-equilibrium effects for NPP operation, as any loss of coolant sustained controls the heat transfer within the core. The overall prediction of this critical flow can drastically improve the safety and integrity of plant.

Leak rate analysis of degraded SG tubes has currently attracted interest of many researchers. Most studies of subcooled critical flow are not indicative to SG tube defect geometries. In the scope of this research, only studies on slit and crack geometries are mentioned. An experimental study, reported by Agostinelli et al., [17], was done with annular, constant area passages with hydraulic diameters ranging from 0.15 to 0.43 mm. The experiment was conducted with water under pressures ranging from 3.5 to 20.5 MPa and subcooling from 9.3^0C to 67^0C. Simoneau, [18], performed a two-phase choked flow experiment with subcooled nitrogen flowing through a slit.

The slit, a narrow rectangular passage of equal length and width, had the L/D (length to diameter ratio) of 43.5. The stagnation pressures were in a range up to 6.8 MPa and inlet temperature was studied over a range $0.84 < T_R < 1.03$, where T_R is the ratio of inlet temperature to critical temperature. Abdollahian et al., [4], carried out a study on two-phase critical (choking) flow through simulated and actual cracks. The experimental results were then used to validate the Battelle critical flow model and recommendations were made to improve the modelling assumptions. The experimental database was then developed by Collier et al. [7]. The study was focused on the effect of fluid pressure and temperature, crack geometry, and crack surface roughness on the leak flow rate. The study used simulated cracks in which geometric conditions were carefully controlled and real intergranular stress corrosion cracks. This study is an effort to build upon previous studies within the multi-phase fuel cell research group at Purdue by Wolf and Vadlamani [19]. A comprehensive review of the above-mentioned studies is tabulated in Table 1.1 below.

Table 1.1 Parameter range of choked flow experiments on slit and crack geometry

Authors	Geometry	L	t X w	Dh	Area	L/D	R	P	ΔTsub
	fluid	[mm]	[mm] x [mm]	[mm]	[mm^2]		roughness [μm]	[Mpa]	[K]
Agostinelli et. Al (1958)	annulus (slit) /steam-water	152-254	(0.15-0.43) X (78.4-79.3)	0.3-0.86	12-38	176-840	(----)	3.5-20.51	10-67
Ryley & Parker (1968)	slits /steam	35.6	(1.27) X (25.4)	2.42	32.3	14.7	(----)	0.008-0.017	0-
Simoneau (1974)	slits /cryogenic N_2	25.4	(25.4)X (0.284-0.3)	0.58	7.42	43.5	(----)	P_{max}=6.8	(----)
Collier et al. (1980)	slits /steam-water	60-75	(0.2-1.12) X (57.2)	0.4-2.2	11.4-64	27-187	0.3-10.2	P_{max}=11.5	33-120
Abdollahian, Levy, Chexal (1983)	cracks /steam-water	18.6-57.2	(0.74-63.5) X (0.0183-1.12)	0.03-1.9	0.015-71.1	30-634	0.3-10.2	3.26-11.53	1-119
Amos & Schrock (1983)	slits /steam-water	63.5	(0.127-0.381) X (14.8-20.5)	0.16-0.77	2.6-7.8	83-400	(----)	4.1-16.2	0-65
Collier et al. (1984)	cracks /steam-water	20	(0.02-0.22) X (0.74-27.9)	0.04-0.44	0.015-6.55	45-500	1.78	P_{max}=11.5	0-72
Kefer et al. (1986)	slits/cracks /steam-water	10-33	(0.097-0.325) X (19-108)	0.26-0.64	5.89-13.93	15-127	20-40	P_{max}=16.0	0-60
John et al. (1987)	slits /steam-water	46	(80)X (0.2-0.6)	0.4	20.0-51.2	115	5-240	4.0-14.0	3-60
Bandyopadhyay et al. (2007)	slits/cracks /steam-water	8	(0.27-0.50) X (15-43.73)	0.54-0.97	5.7-11.8	8.3-14.8	(----)	1.14-8.66	58-264
Wolf & Revankar, (2012)	slits/steam-water	3.175	(0.25-0.50)X(2.4-3.2)	0.55-0.84	0.86-1.92	4.48-6.94	30	6.89	24-46
Vadlamani & Revankar, (2013)	slits/steam-water	1.3	(0.83-2.6)X(0.285-0.648)	0.61-1.04	0.513-4.59	1.2-2.1	5-30	6.895	14.1-49.1

1.3.1 Homogeneous Equilibrium

The homogeneous equilibrium model (HEM), is the only completely theoretical critical flow model. HEM ignores slip and non-equilibrium effects. One assumes the flow is steady, the two phases flow with the same velocity, no slip between phases, thermal equilibrium between phases, isentropic expansion, and the body forces, chemical reactions, and friction are neglected [16]. According to these assumptions, this two-phase mixture can be represented as a single-phase flow. Thus, the choking mass flux dependence is on upstream conditions. Maximizing G is done with respect to pressure resulting in Equation 1.1. Solutions of mixture conservation equations and the constraint of equation 1.1 shows the critical flow velocity is ultimately the homogeneous equilibrium sound speed represented by Equation 1.2 [5].

$$\frac{dG}{dP} = 0 \tag{1.1}$$

$$v_{ex} = a_{HE} = \left(\frac{dP}{d\rho}\right)^{\frac{1}{2}} \tag{1.2}$$

It is possible at a subcooled stagnation state the mixture velocity exceeds the homogeneous equilibrium sound speed with zero quality; however, for single-phase supersonic flow, a convergent/divergent nozzle is necessary and cannot occur in a straight duct (i.e. SG cracks). Insufficient time to establish mechanical equilibrium becomes a limitation of accurately applying the HEM model to short channels; therefore, the HEM model shows promise for long channels where mechanical equilibrium has been established under stagnation conditions [16].

Phase change in a flow channel is driven by three mechanisms: area change, friction, and heat addition. In the case of short channels, rapid depressurization is attributed for the phase change; however, without friction or heat addition there can be no phase change. This results in an underestimated choking flow rate in short channels.

1.3.2 Homogeneous Non-Equilibrium

Homogeneous non-equilibrium (HNEM) two-phase critical models assume that between two-phases, gas and liquid, there is no presence of thermal equilibrium. It is acknowledged for short channels the local heat and mass transfer rates at the throat can be large for initially subcooled liquids. Henry and Fauske noticed this discrepancy and believed thermal non-equilibrium effects

were more significant than those of slip. This resulted in an empirical non-equilibrium parameter N, which represents the partial phase change at the throat [1], [2]. Their simplified critical mass flux is given by [20],

$$G_c^2 = \left[\frac{x_o}{np\rho_g} + \left(\frac{1}{\rho_g} - \frac{1}{\rho_{L0}}\right)\left\{\frac{(1-x_o)N}{s_{GE} - s_{LE}}\frac{dS_{LE}}{dp} - \frac{x_o C_{P_G}\left(\frac{1}{n} - \frac{1}{\gamma}\right)}{p(s_{G0} - s_{L0})}\right\}\right]_t^{-1} \tag{1.3}$$

The rate of mass transfer at the throat was correlated to equilibrium value via Equation 1.4.

$$\frac{dx}{dP}|_t = N\frac{dx_E}{dP}|_t \tag{1.4}$$

x_{eq} and $\frac{dx_{eq}}{dP}$ were calculated based on an isentropic process. x_{eq} and x are given as,

$$x_{eq} = \frac{s_0 - s_L}{s_G - s_L} \tag{1.5}$$

$$x = Nx_{eq}, where\ N = \begin{Bmatrix} nx_{eq}\ x_{eq} \le \frac{1}{n} \\ 1.0\ x_{eq} > \frac{1}{n} \end{Bmatrix} \tag{1.6}$$

The model can be further simplified for case where x_0 is equal to zero or unity. The critical expression is reduced to the following Equation 1.7 and the non-equilibrium parameter takes the form of Equation 1.8. This average equilibrium quality was correlated from the work of Starkman et al. experiments [21].

$$G_c^2 = \left[\left(v_{gE} - v_{l0}\right)\frac{N}{s_{gE} - s_{lE}}\frac{ds_{lE}}{dP}\right]_t^{-1} \tag{1.7}$$

$$N = \frac{x_{eq_t}}{0.14}$$

The model of Levy and Abdollahian, [22], takes a less arbitrary approve of identifying the presence of metastable liquid phase [5]. Prediction of pressure at the point of flashing is correlated from the pressure undershoot correlation of Alamgir-Lienhard [23]. The assumption of isentropic flow allows the mixture energy equation of homogeneous flow to be used for the solution of mass flux given by Equation 1.8.

$$G_c^2 = \frac{2}{v^2}\left[h_0 - (1-x)h_f - xh_g\right] \tag{1.8}$$

1.3.3 Non-Homogeneous Equilibrium

Non-homogeneous equilibrium (NHEM) models are based on slip ratio between the two phases. This is done by taking the ratio of gas and liquid phase velocities. There are three well known models each having their own respective shortcomings. These are the models developed by Fauske, Levy, and Moody [24]–[26]. Fauske's approach to the slip ratio failed to conserve energy as did Levy's, whereas Moody failed to conserve momentum.

Due to the missing conservation equations the nature of the flow must be assumed. Moody required the mass flux to be maximum with respect to slip ratio, and Fauske assumed the pressure gradient was maximum at the choking plane respective to the slip ratio. Levy derived separate conservation equations of mass and momentum for each phase. Each model's predictions of the slip ratio by the above-mentioned authors are larger than any experimentally observed.

1.3.4 Non-Homogeneous Non -Equilibrium

Non-homogeneous non-equilibrium (NHNEM) models are intuitive. It is readily easy to visual the mechanical and thermal non-equilibrium characteristics; however, mathematical representation proves challenging. The two-fluid model considers simultaneous non-equilibrium. This model requires separate constitutive relations for each phase and interaction terms for interphase heat, mass, and momentum transfer [27]. These conservation equations can be seen in detail through the work of Ishii, [28]. Choking flow conditions, where convective acceleration and depressurization takes place, reduces the accuracy of the constitutive relations. Many assumptions need to be made in order to simplify the mathematical complications and uncertainties in specifying interfacial interaction terms of the two phases [29]

2. EXPERIMENTAL PROGRAM

2.1 Experimental Test Facility

The test facility was designed to measure mass flow rate of water leaking through the SG tube cracks. It is modular so that various crack geometries can be studied. The pressure differential across the tube wall can be increased up to 6.89 MPa (1000 psi). A vertical pressure vessel used as a blowdown tank was constructed from a single seamless pipe of Schedule 160 316 SS. The vessel has a diameter of 90 mm (3.5 in) and was tested at 14 MPa (2000 psi), which is double the maximum operating pressure to ensure safety. A pressure relief valve is installed on the top of the vessel, which will open at the onset of system pressure 8.3 MPa (1204 psi). The vessel is connected to a compressed nitrogen cylinder through 9.5 mm stainless steel tubing. Since the experiment was conducted at high pressures and temperatures, three ceramic band heaters are used to heat the pressure vessel from the outside. Each heater can produce 1200 W and they are wired in parallel for operation at 240 V. Pressure and temperature of the liquid were measured before it flows into the test section. The discharge steam is condensed by a cold-water tank where the outlet of the test section is submerged. The tank was suspended from two loads cells via steel cables. The mass of the tank measured by the load cells was used to calculate the discharge mass flow rate. The load cells signal was amplified and transmitted to a data acquisition system.

The water level in the pressure vessel was measured by a Honeywell differential pressure (DP) transducer. A needle gauge was installed to monitor the pressure in the vessel during a test. A gauge pressure transmitter was used to measure the pressure before the test specimen. The temperature was measured by K-type thermocouples installed along the pressure vessel and before the test specimen as shown in Fig. 2-1. All thermocouples were inserted to the centerline of flow at their respective locations. The mineral wool insulation, which has a thickness of 5.08cm (2 in), was used to reduce heat loss from the vessel during heating of the water. The load cells, differential pressure transducer and thermocouples were connected to the data acquisition system. A Labview program was developed to record and display the data in real time for monitoring. Thermocouples data were taken at 1 Hz while all the other data were recorded at 100 Hz.

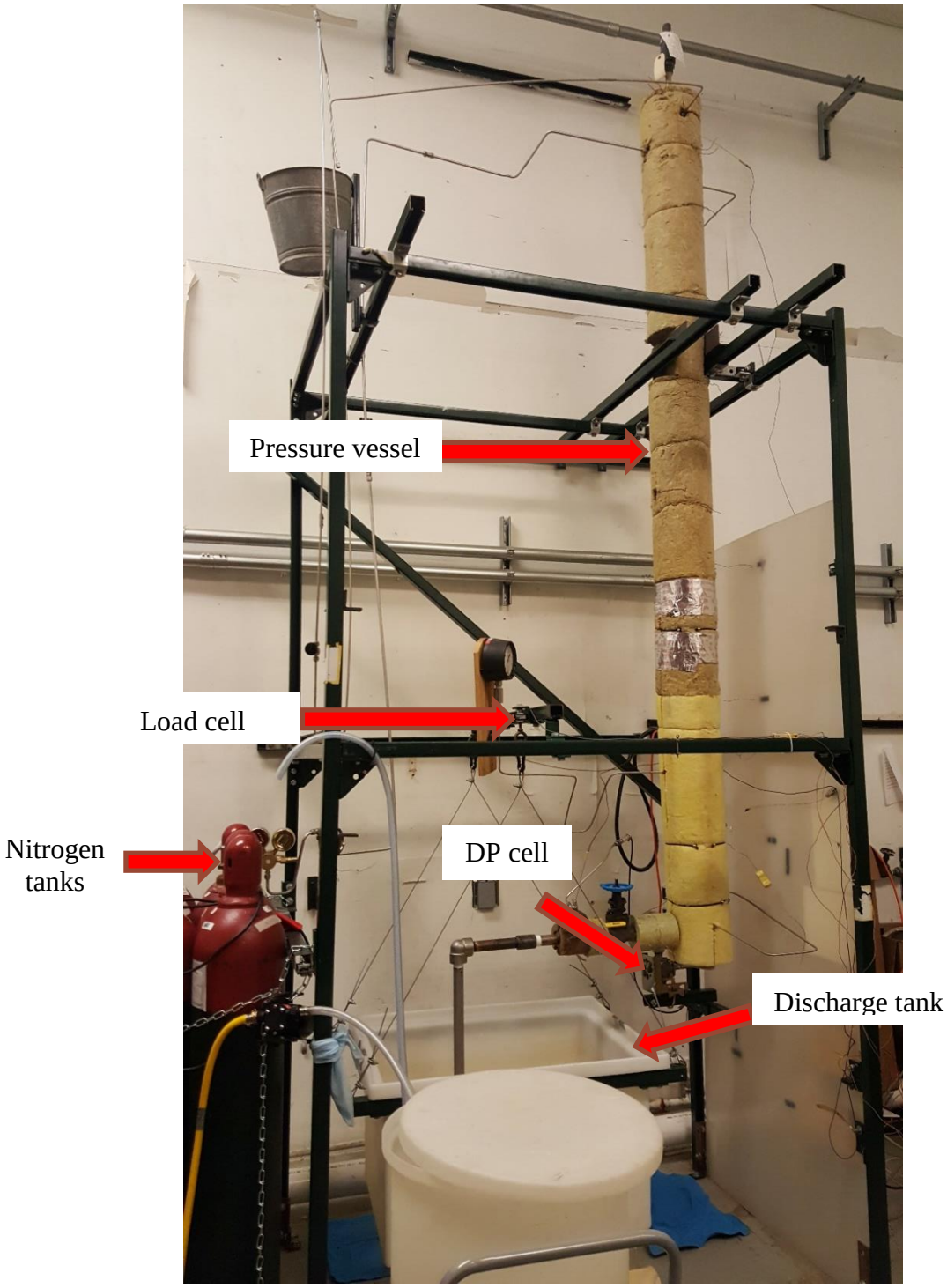

Figure 2-1 Experimental test facility assembly

2.2 Crack Sample Fabrication

Six samples of simulated SG tubes studied in this work are numbered from 6-11. The smooth crack surfaces were achieved by welding 2 semicircular halves of 49-gauge 316 SS sheet to a 304 SS schedule 40 nipple. The gap between them is set via a feeler gauge with an accuracy of 0.0001". The length of the slit is filled to desired specifications by welding the semicircular halves together. For example, samples 6-8 were to have similar area with incremental L/D only due to decreasing hydraulic diameter, and samples 9-11 were to have similar area with varying L/D only due to decreasing hydraulic diameter. Due to the nature of welding, the width of the crack varies, and the overall exit area was deemed to be inconsistent for each group of samples (i.e. samples 6-8 and samples 9-11).

Figure 2-2 Slit Samples 6, 7, and 8.

Figure 2-3 Slit samples 9, 10, 11.

2.2.1 Crack Area Measurement

In order to calculate the discharge mass flux, the dimensions of each crack must be measured. In this research, a microscope is used to obtain the crack's dimensions. Magnification of the microscope was set at different values depending on the dimensions of crack samples. The lowest and highest magnification used are 1.5 and 6. Prior to the heated experiment, the test specimens were put in a high-pressure cold-water test at 6.89 MPa, which is the maximum stagnation pressure in the experiment. The areas of the cracks were measured before and after the test to evaluate material expansion under the high pressure. The test was repeated until no further increase in the areas could be detected. The final value of the area measurement was used throughout the experiment. The images are processed by Photoshop program and Matlab to identify the areas and L/D ratios. The procedure to do this task is shown as follow:

- An image taken by the microscope is loaded into Photoshop program. The area of crack is selected using the software tools. The selected area is filled with white color to make a uniform color throughout the crack. The purpose of this work is to prepare the image for Matlab processing.

- The image (gray-scale) is loaded into Matlab program. It is then converted to a binary image (only black and white colors) using Matlab commands.
- Now the image is ready for counting white pixels; however, one more step is needed to calculate perimeter. Using the algorithm within Matlab, the program can display only the pixels lying on the perimeter of the crack.
- To calculate the area, the total number of white pixels in the binary image is counted. To calculate the perimeter, the number of white pixels on the crack's perimeter is counted. Another image of the same magnification was taken with a scale to calculate dimension of each pixel. Crack's area and perimeter can be used to determine crack's hydraulic diameter.

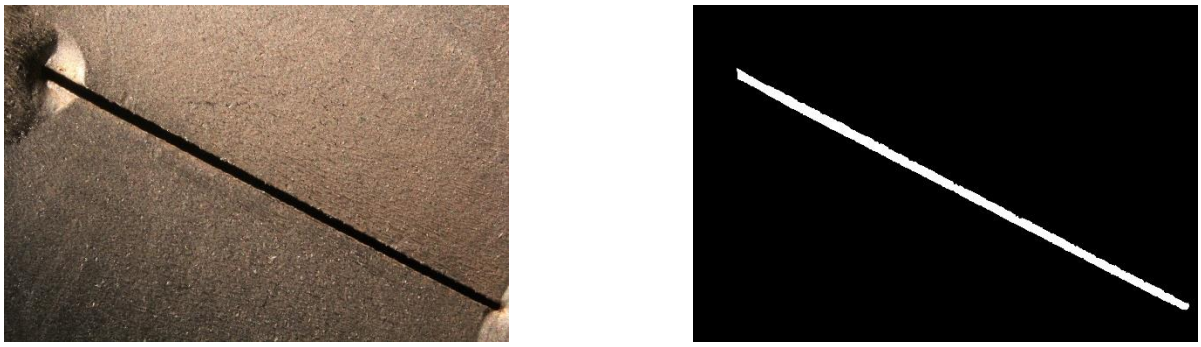

Figure 2-4 Original (left) and processed (right) image of a crack

Table 2.1 Dimensions of the samples' cracks

No of sample	Opening Area (m^2)	Length of Channel, L(m)	Hydraulic Diameter, D(m)	L/D
6	2.280E-06	1.140E-03	3.813E-04	3.0
7	2.277E-06	1.140E-03	3.526E-04	3.2
8	2.493E-06	1.140E-03	3.223E-04	3.5
9	1.997E-06	1.140E-03	3.074E-04	3.7
10	1.337E-06	1.140E-03	2.161E-04	5.3
11	2.492E-06	1.140E-03	2.675E-04	4.3

2.3 Test procedure

The following outlines the experimental procedures for operation of the leak rate facility.

I. Ensure water used in the facility is de-ionized water.

II. Condensing tank must be filled with water above the outlet section by ~ 2".

III. Make sure each power supply is zeroed out prior to powering. The excitation for the Load Cells (LC) is 10.2 V and for the DP Transducer and DP transmitter 24.2 V. Plug in the digital thermocouple display and amplifier. Open LabView to observe instrumentation feedback.

IV. Prior to filling make sure the gate valve, fill valve, and vent line are open.

V. Attach the fill line and prime the utility pump prior to filling the pressure vessel.

VI. The gate valve and fill valve are closed, and the pump is power off once desired water level is reached (~ 4.2 V). The vent line is closed and bleed the DP Transducer high/low side.

VII. For non-heating experiments, the vent line remains closed and the nitrogen regulator is opened to obtain the desired test pressure. For heating experiments, the vessel is pressurized to 60 psi and the heaters are plugged in. The water is allowed to reach saturation temperature. The regulator is closed, and the vent line is opened to degas the system.

VIII. Close the vent line and open the nitrogen regulator to increase the system pressure to 100 psi. Increasing the system pressure by 100 psi until desired overall pressure is met.

IX. Once the desired temperature and pressure are met, turn off the band heaters and start the data acquisition. Open the gate valve.

X. Once the water level is near the bottom of the vessel (~1.9 V), stop the data acquisition. Close the nitrogen regulator and gate valve as quickly as possible.

XI. Open the vent line to relieve the remaining pressure in the system. Once the pressure has dropped to ~200 psi, open the gate valve. After all the pressure has been relieved open the

fill valve. All valves after a heated test should remain open to prevent steam pressurization within the system.

XII. Doors to the facility are then opened to allow adequate air ventilation in the area.

2.4 Reduction of Raw Data

Two independent mass measurements are recorded and averaged to determine an overall mass flow rate. As previously discussed, a DP transducer is used to monitor water level within the pressure vessel, and load cells record the mass feedback of the condensing tank. Mass flow rate is computed by the changing water level. once the pressure profile is constant represented by Fig 2-5. The change of densities of both water and nitrogen are considered. The mass of the metastable discharge is recorded at a rate of 100/second and averaged every 10 data points. A plot of this data can be seen in Fig. 2-6.

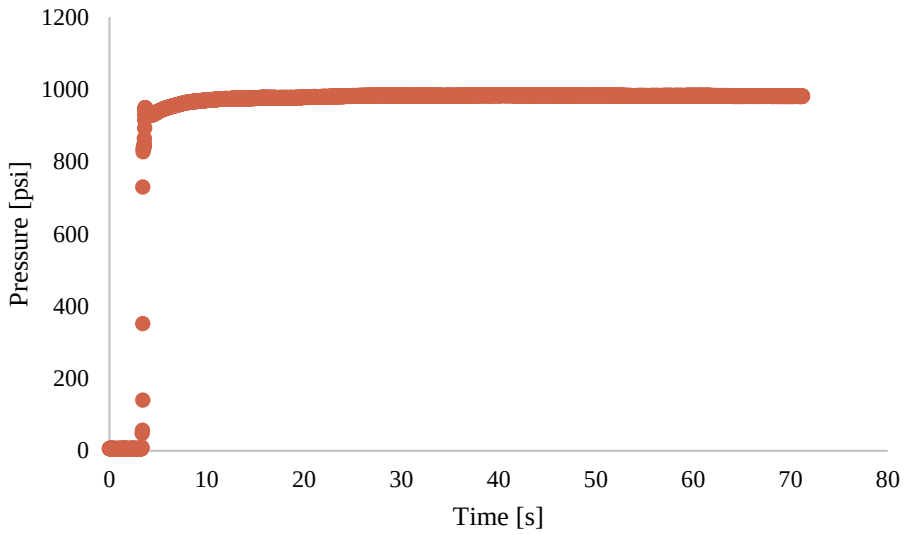

Figure 2-5 Steady state pressure profile

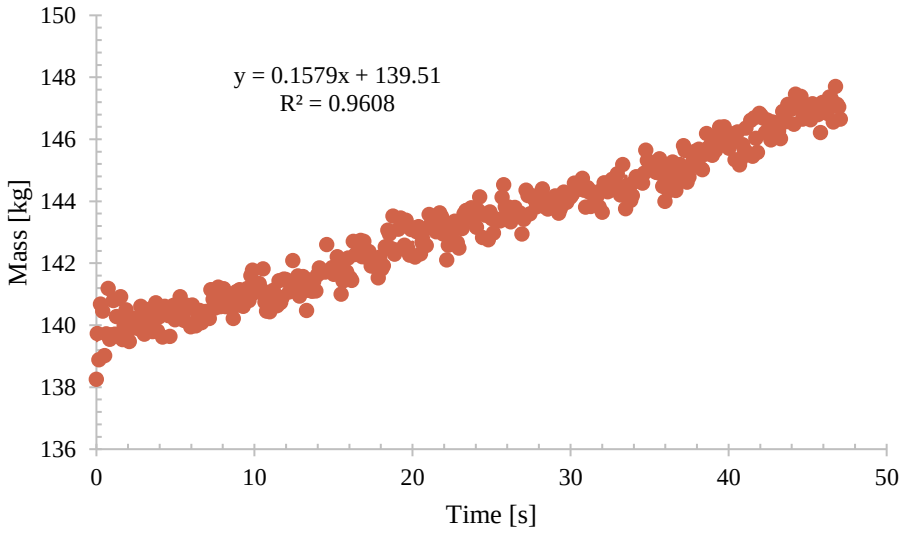

Figure 2-6 Load cell mass feedback

2.5 Experimental Results

2.5.1 Room Temperature Discharge Tests

The tests were carried out at room temperature (20^0C). This flow rate data was used to calculate Reynolds number and discharge coefficients for each simulated steam generator tube crack sample. The water is discharged to atmospheric pressure conditions; thus, upstream pressure becomes the total pressure drop (ΔP) across the crack. The Reynolds number (Re) and discharge coefficient (C_d) are calculated as follow:

$$Re = \frac{GD}{\mu} \tag{2.1}$$

$$C_d = \frac{G}{\sqrt{2\rho\Delta P}} \tag{2.2}$$

Results of Re and C_d calculation are presented in Tables 2.2-2.7 for each sample. Correlations between the discharge coefficient and Reynolds number for crack samples are shown in Figure 2.7 to 2.12.

Table 2.2 Room temperature discharge test result for sample 6

P (MPa)	m (kg/s)	G (kg/m^{2}s)	Re	C_d
0.686	0.07	3.36E+04	1.17E+04	0.87
1.341	0.10	4.61E+04	1.61E+04	0.85
2.709	0.14	6.50E+04	2.24E+04	0.84
4.112	0.17	7.78E+04	2.69E+04	0.82
5.426	0.19	8.84E+04	3.05E+04	0.81
6.484	0.21	9.44E+04	3.26E+04	0.79

Table 2.3 Room temperature discharge test result for sample 7

P (MPa)	m (kg/s)	G (kg/m^{2}s)	Re	C_d
0.672	0.07	3.06E+04	9.30E+03	0.83
1.413	0.10	4.55E+04	1.38E+04	0.85
2.728	0.14	6.12E+04	1.84E+04	0.83
3.960	0.17	7.50E+04	2.25E+04	0.84
5.441	0.19	8.54E+04	2.57E+04	0.82
6.795	0.22	9.52E+04	2.86E+04	0.82

Table 2.4 Room temperature discharge test result for sample 8

P (MPa)	m (kg/s)	G (kg/m^{2}s)	Re	C_d
0.794	0.05	1.93E+04	7.51E+03	0.48
1.492	0.07	2.88E+04	1.11E+04	0.53
2.843	0.10	4.04E+04	1.55E+04	0.54
4.038	0.12	4.66E+04	1.79E+04	0.52
5.510	0.14	5.56E+04	2.13E+04	0.53
6.550	0.15	5.89E+04	2.26E+04	0.52

Table 2.5 Room temperature discharge test result for sample 9

P (kPa)	m (kg/s)	G (kg/m^{2}s)	Re	C_d
0.752	0.06	2.33E+04	8.65E+03	0.60
1.547	0.08	3.28E+04	1.22E+04	0.59
2.875	0.12	4.52E+04	1.68E+04	0.60
4.061	0.16	7.92E+04	2.48E+04	0.88
5.349	0.18	8.97E+04	2.81E+04	0.87
6.659	0.20	9.90E+04	3.10E+04	0.86

Table 2.6 Room temperature discharge test result for sample 10

P (MPa)	m (kg/s)	G (kg/m^{2}s)	Re	C_d
0.705	0.04	3.18E+04	4.74E+03	0.85
1.420	0.06	4.72E+04	7.03E+03	0.89
2.676	0.09	6.64E+04	9.79E+03	0.91
4.054	0.11	8.40E+04	1.24E+04	0.93
5.408	0.13	9.95E+04	1.47E+04	0.96
6.916	0.16	1.16E+05	1.71E+04	0.99

Table 2.7 Room temperature discharge test result for sample 11

P (MPa)	m (kg/s)	G (kg/m^{2}s)	Re	C_d
0.684	0.07	2.92E+04	4.35E+03	0.79
1.483	0.11	4.43E+04	6.60E+03	0.81
2.743	0.15	6.11E+04	9.01E+03	0.83
4.054	0.18	7.37E+04	1.09E+04	0.82
5.328	0.21	8.52E+04	1.26E+04	0.83
6.727	0.23	9.32E+04	1.37E+04	0.80

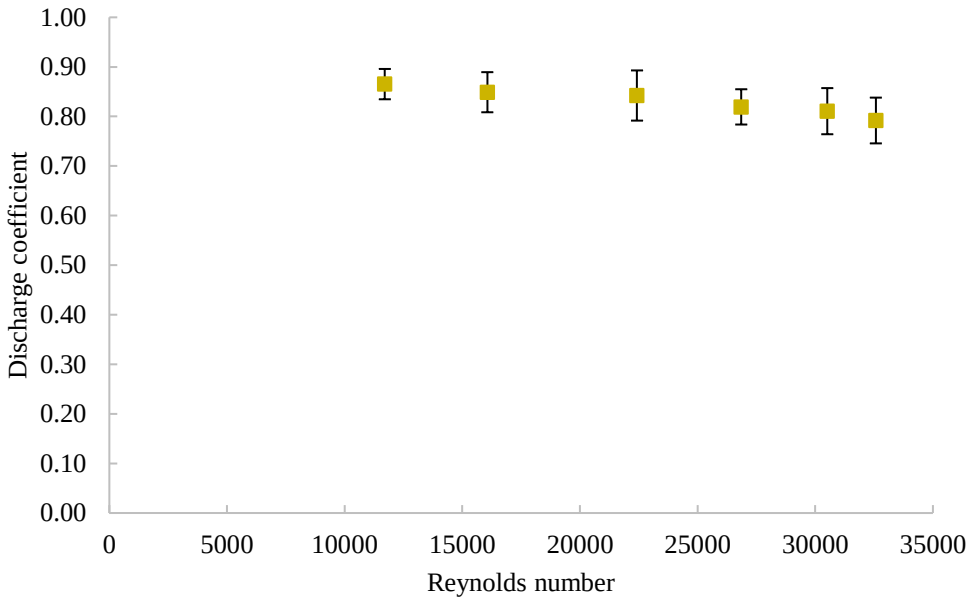

Figure 2-7 Discharge coefficient for Sample 6

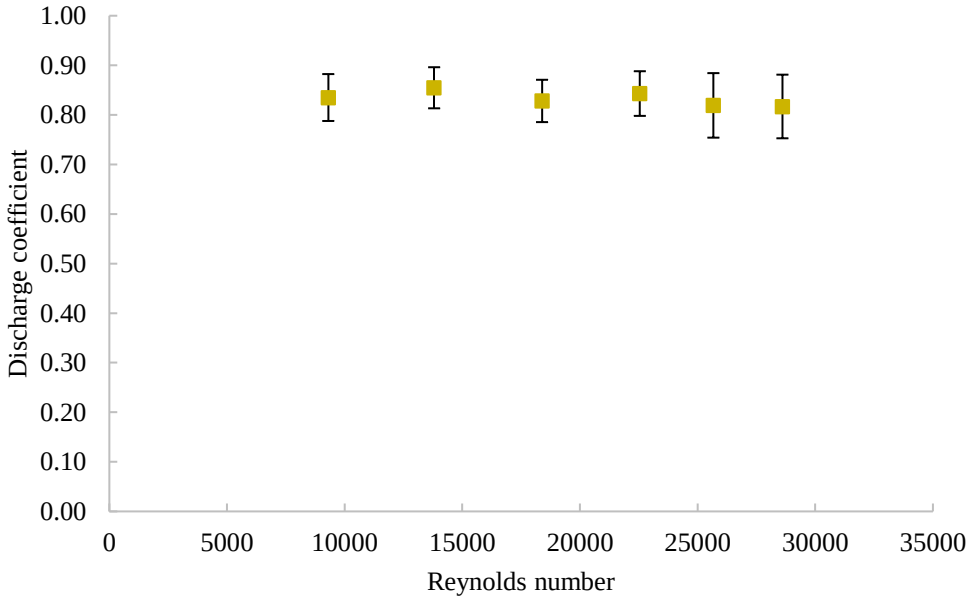

Figure 2-8 Discharge coefficient for Sample 7

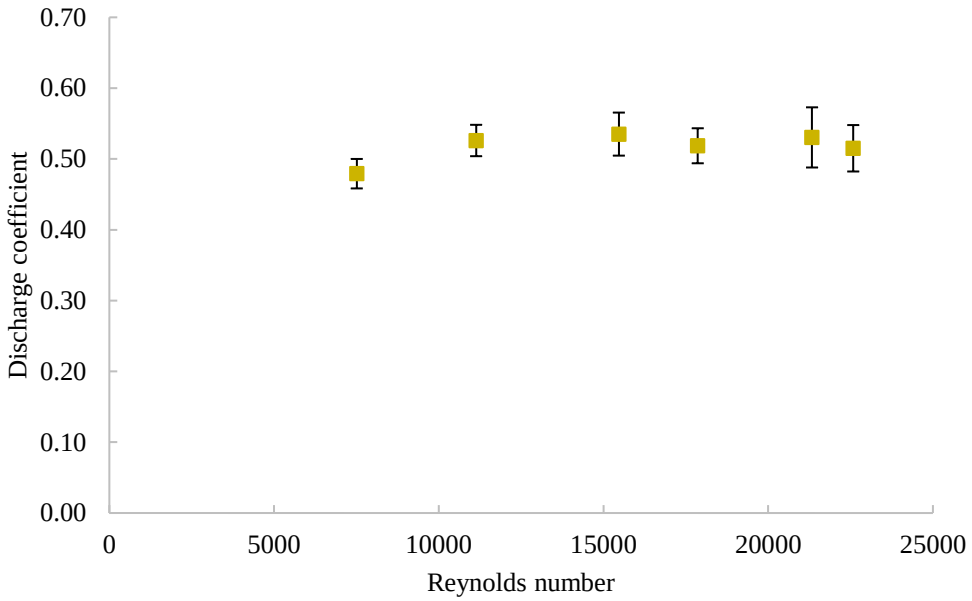

Figure 2-9 Discharge coefficient for Sample 8

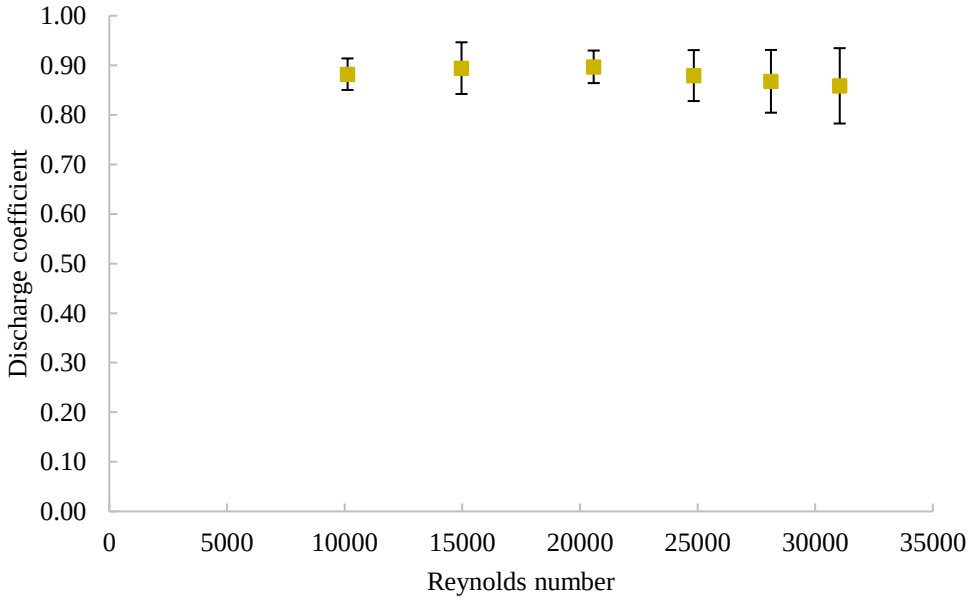

Figure 2-10 Discharge coefficient for Sample 9

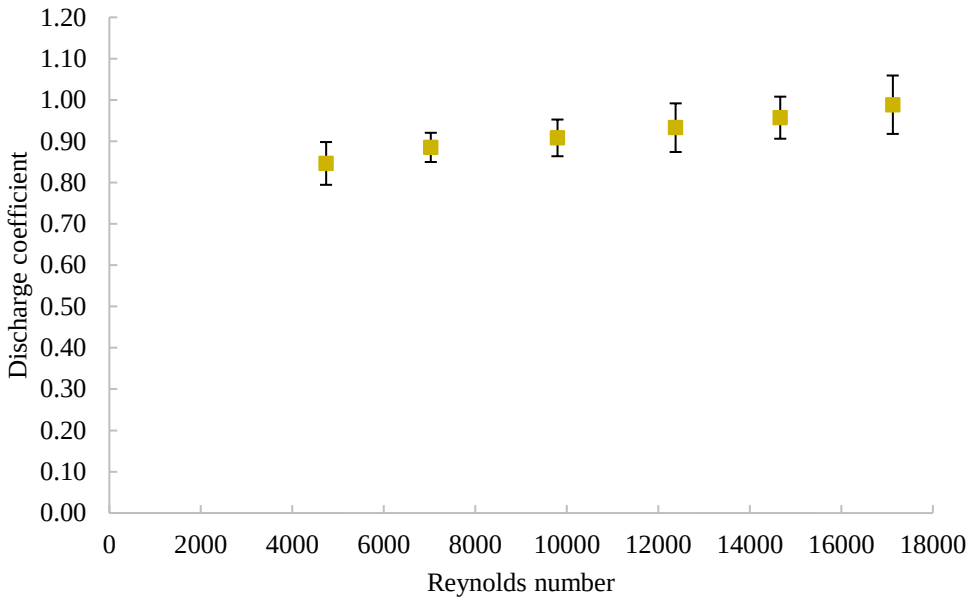

Figure 2-11 Discharge coefficient for Sample 10

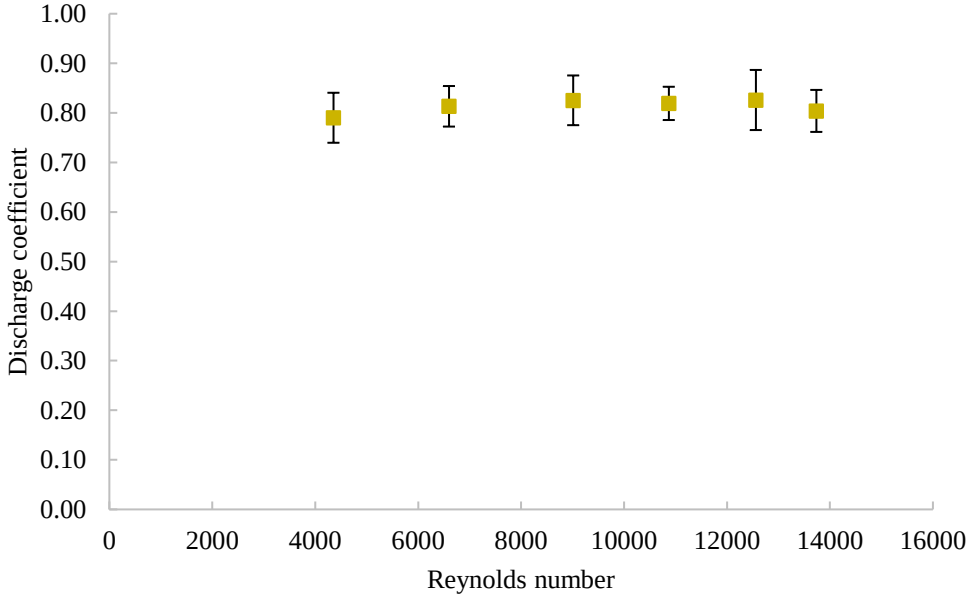

Figure 2-12 Discharge coefficient for Sample 11

2.5.2 Effect of Liquid Subcooling

Effect of liquid subcooling on the choking mass flux is assessed by conducting the subcooled flashing test at a fixed the stagnation pressure. The liquid subcooling is up to 80℃ and the test was performed at two stagnation pressures 6.89 MPa (600 psi) and 4.14 MPa (600 psi). It is shown that behavior of the mass flux with respect to the subcooling is similar for various test specimens. As would be expected, at a fixed stagnation pressure, the highest mass flux for each crack sample was obtained at the highest subcooling, along with the lowest mass flux for the lowest subcooling.

As the subcooling increases, the flashing location should move closer to the channel exit and less vapor would be generated due to liquid flashing. Since two-phase frictional pressure drop is generally higher than that for a single-phase flow at the same mass flux, the relocation of flashing point and decrease in vapor quantity should lead to an increase in the mass flux for a fixed stagnation pressure.

The results have been presented in tabular form followed by a plot examining the influence of subcoolings on mass flow rates for each sample studied.

Table 2.8 Subcooled flashing discharge test results Sample 6

P (MPa)	Subcooling (C)	G (kg/m^{2}s)
6.76E	80.1	8.24E+04
7.08	63.2	7.68E+04
6.92	43.3	6.75E+04
6.55	18.6	6.40E+04
4.11	65.7	5.77E+04
4.16	53.5	6.38E+04
4.11	35.0	5.93E+04
4.17	25.0	5.45E+04

Table 2.9 Subcooled flashing discharge test results Sample 7

P (MPa)	Subcooling (C)	G (kg/m^{2}s)
6.89	78.2	8.37E+04
7.23	64.9	8.26E+04
6.88	41.9	7.78E+04
7.05	23.5	6.74E+04
4.20	67.0	6.73E+04
4.12	49.0	6.49E+04
4.21	32.2	5.90E+04
4.17	25.5	5.98E+04

Table 2.10 Subcooled flashing discharge test results Sample 8

P (kPa)	Subcooling (C)	G (kg/m^{2}s)
6.77	80.0	6.04E+04
6.94	63.2	5.97E+04
6.95	41.5	5.80E+04
6.84	21.6	5.51E+04
4.15	69.3	4.83E+04
4.18	50.1	4.71E+04
4.16	31.5	4.36E+04
4.16	23.3	4.17E+04

Table 2.11 Subcooled flashing discharge test results Sample 9

P (MPa)	Subcooling (C)	G (kg/m^{2}s)
6.98	81.7	9.49E+04
6.84	59.2	8.85E+04
6.85	43.7	8.08E+04
6.90	21.9	7.08E+04
4.13	54.6	6.93E+04
4.09	49.2	6.70E+04
4.08	34.4	6.22E+04
4.14	21.7	5.83E+04

Table 2.12 Subcooled flashing discharge test results Sample 10

P (MPa)	Subcooling (C)	G (kg/m^{2}s)
6.92	82.6	1.14E+05
6.99	63.4	1.15E+05
6.92	41.4	9.73E+04
7.20	25.6	9.24E+04
4.11	67.7	8.64E+04
4.13	50.1	8.22E+04
4.16	35.4	7.44E+04
4.12	34.8	7.11E+04

Table 2.13 Subcooled flashing discharge test results for Sample 11

P (MPa)	Subcooling (C)	G (kg/m^{2}s)
6.74	79.0	8.60E+04
7.04	60.8	7.98E+04
6.97	41.3	7.24E+04
7.03	22.6	6.64E+04
4.12	65.7	5.83E+04
4.16	53.5	5.84E+04
4.12	35.4	4.85E+04
4.17	22.6	4.76E+04

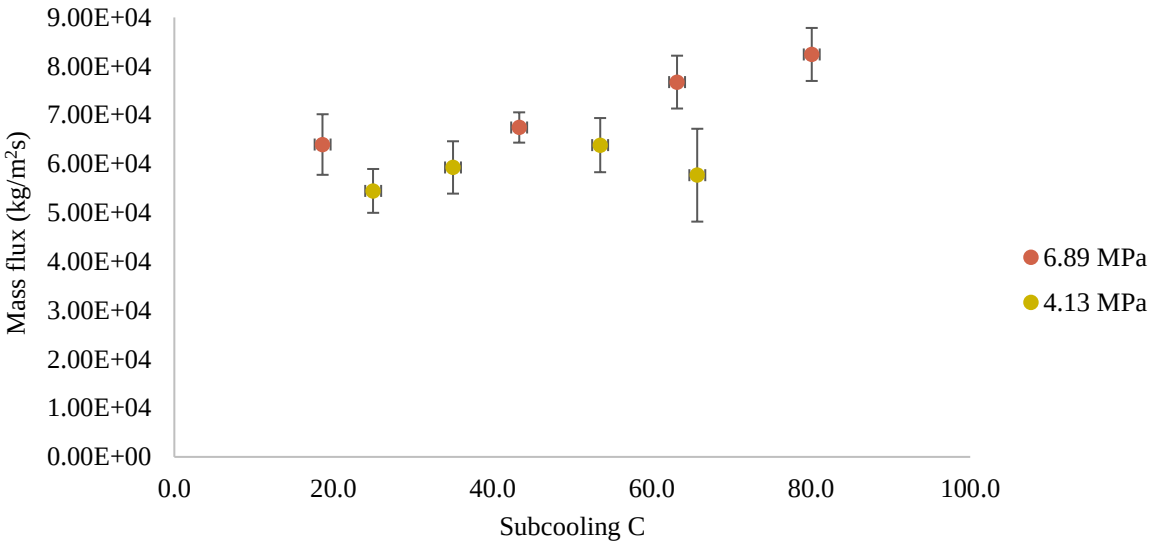

Figure 2-13 Subcooled choking mass flux as a function of subcooling Sample 6

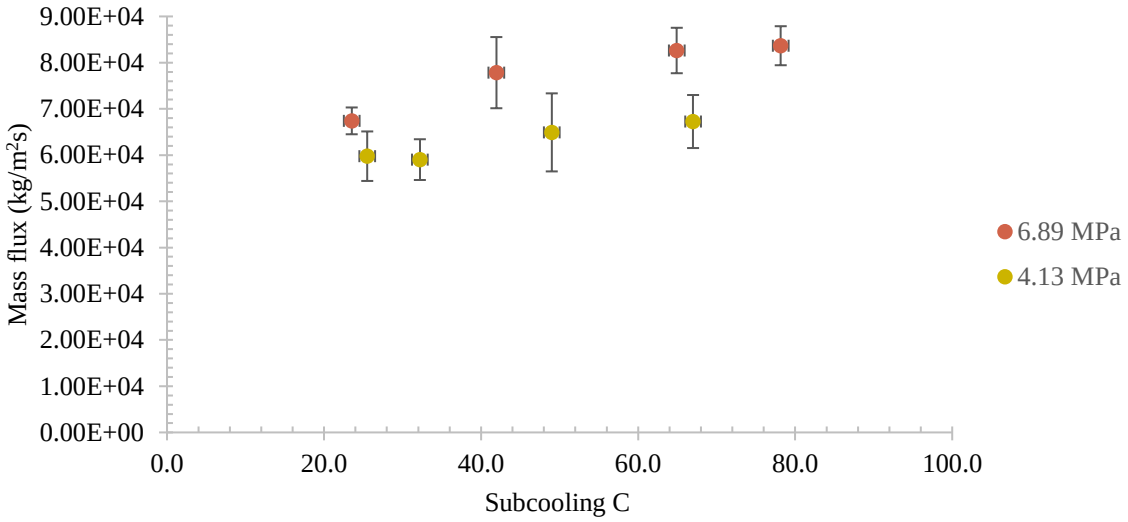

Figure 2-14 Subcooled choking mass flux as a function of subcooling Sample 7

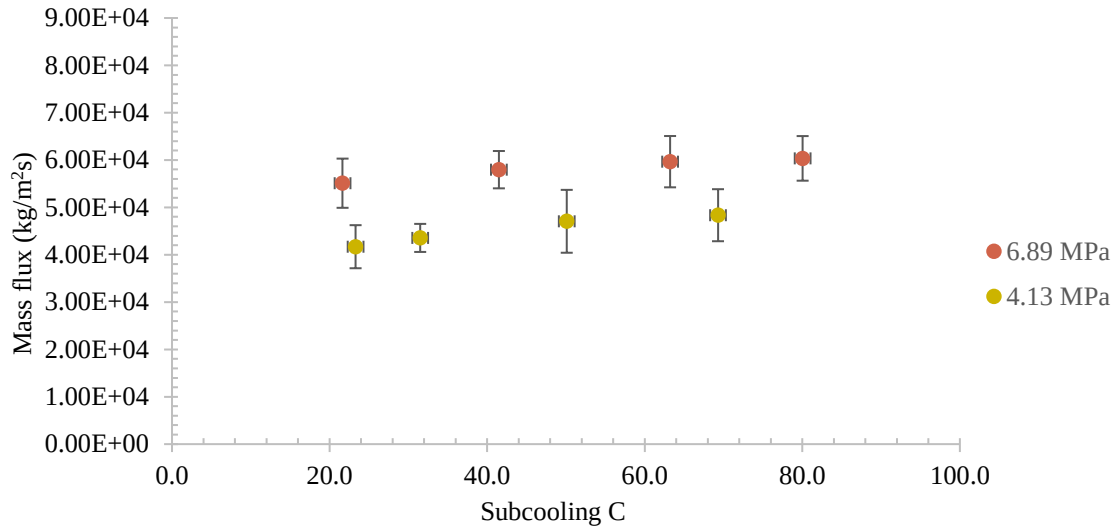

Figure 2-15 Subcooled choking mass flux as a function of subcooling Sample 8

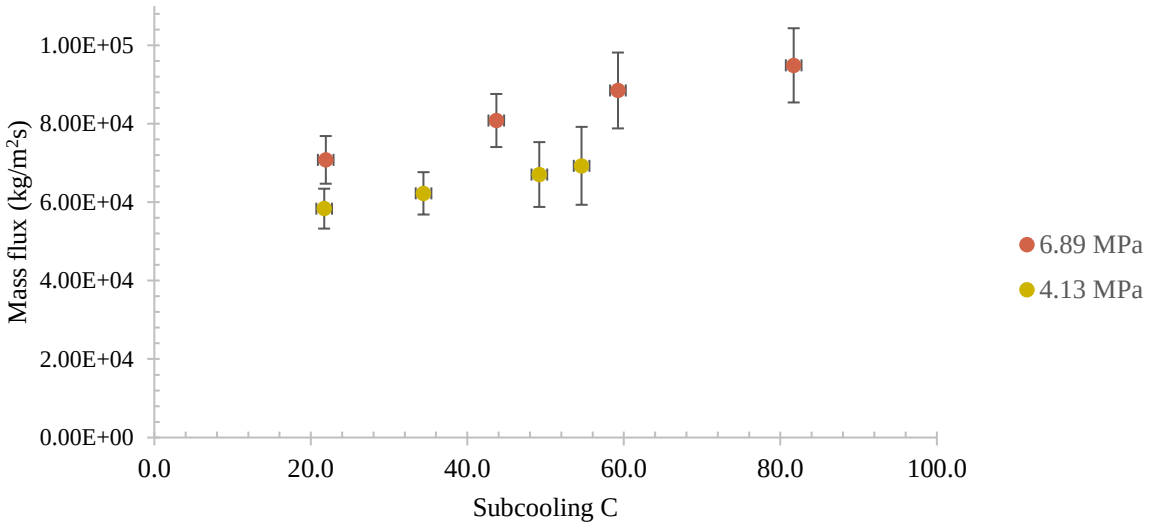

Figure 2-16 Subcooled choking mass flux as a function of subcooling Sample 9

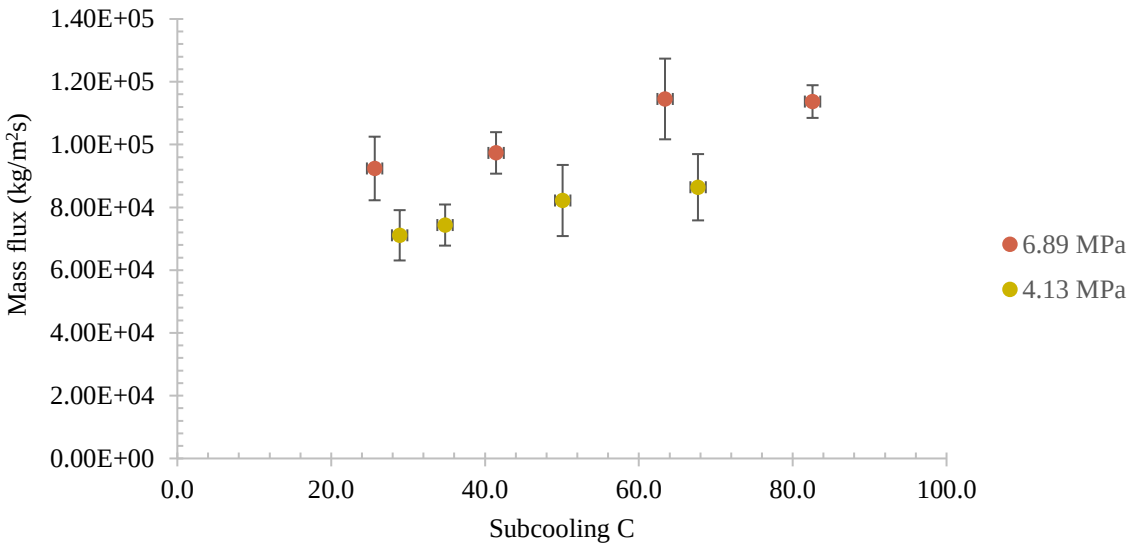

Figure 2-17 Subcooled choking mass flux as a function of subcooling Sample 10

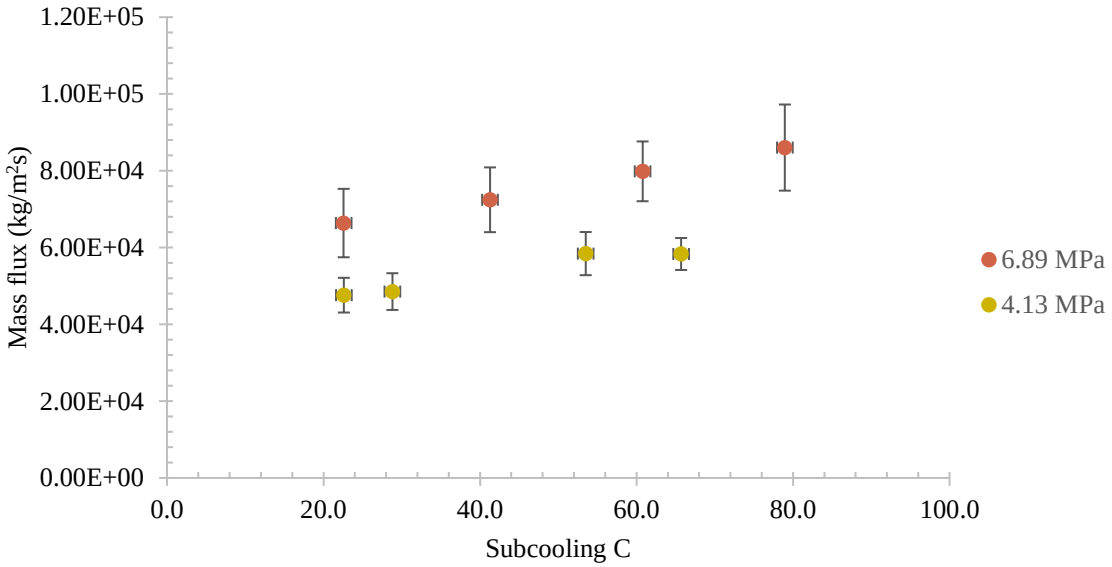

Figure 2-18 Subcooled choking mass flux as a function of subcooling Sample 11

2.5.3 Effect of Stagnation Pressure

The dependence of choking mass flux on stagnation pressure is studied for each sample. In this study, the stagnation pressure was varied from 4.137 MPa (600 psi) to 6.89 MPa (1000psi). As would be expected, the trend of the data is that the mass flux increases with increasing the stagnation pressure. Amos and Schrock, through their observation, showed that the effect of stagnation pressure on the mass flux in the subcooled flashing test changes for different L/Ds. All the data points are chosen such that the liquid subcoolings is about 20℃ to minimize its effect on the mass flux. It is indicated that as the L/D increases due to a decrease in hydraulic diameter, rate of change of the mass flux with respect to stagnation pressure is significantly reduced. Liquid going through a very short channel length is subjected to very high depressurization rate, which makes the liquid superheated and the flashing is delayed. Studies on the choked flow models consider this effect and provide prediction of the choking mass flux significantly affected by the flashing location [5], [30]. More details about the effect of L/D will be discussed in the following section at a fixed stagnation pressure and varying liquid subcooling.

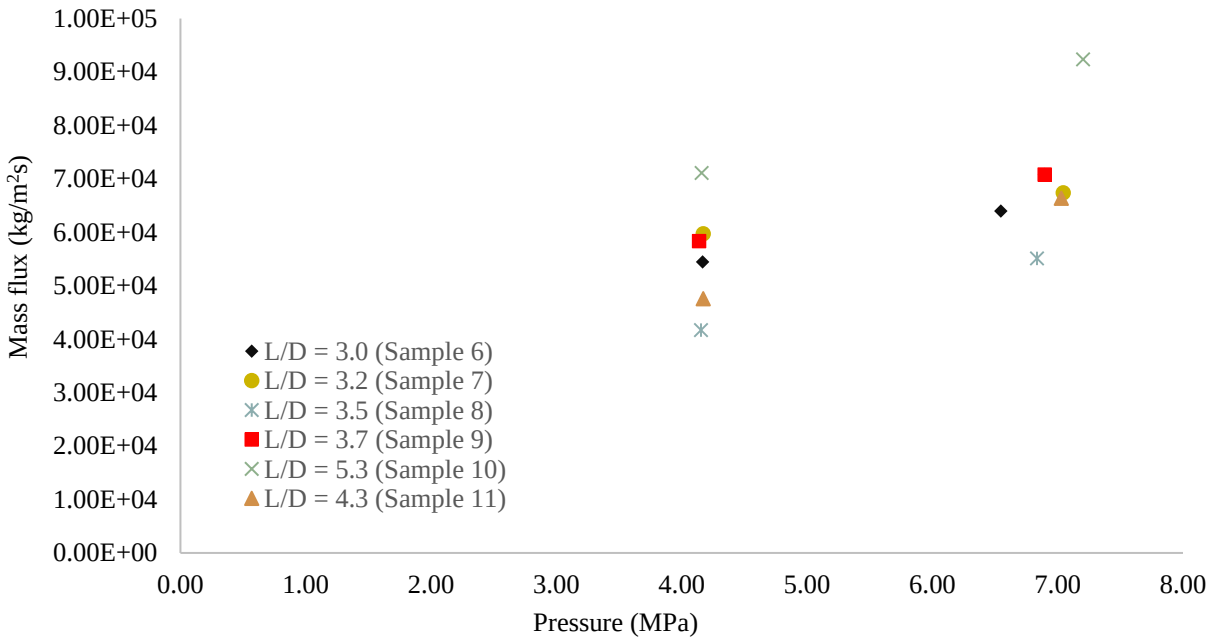

Figure 2-19 Subcooled flashing discharge mass flux at different L/D ratios

2.5.4 Effect of Channel Length to Diameter Ratio

The channel friction has an important effect on the choking mass flux. Pressure drop of the flow due to friction is proportional to fL/D. Therefore, the experiment results in this section are discussed in terms of the length to diameter ratio. The values of this ratio in the current study varies from 3.0 to 5.3. The increase in the length to diameter ratio can be attributed to a decrease of the hydraulic diameter of the channel. Amos and Schrock found that a decrease in the channel hydraulic diameter for a fixed channel length leads to a reduction in the mass flux [5].

The results presented in Figures 2-20 and 2-21 were conducted on smooth slits to avoid large difference in friction factor between the test specimens. The data is grouped with respect to liquid subcooling. For two-phase flow, the dependence of mass flux on the L/D is expected to be stronger due to higher frictional pressure drop. As the L/D increases, more kinetic energy of the flow is lost due to the friction, which leads to the decrease in the mass flux. This isn't observed for the short channel length used in this study. Where areas are similar in the cases of L/D 3.0 and 3.7, the mass flux increases for an increasing L/D. This is again observed for the case of L/D 3.5 and 4.3.

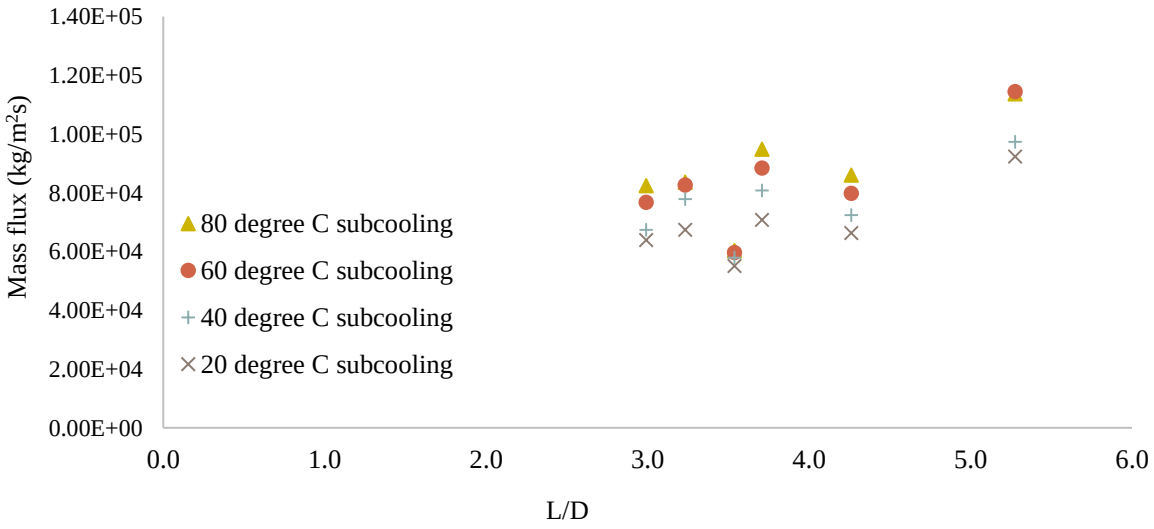

Figure 2-20 Mass flux versus L/D for the subcooled flashing tests at 6.89 MPa

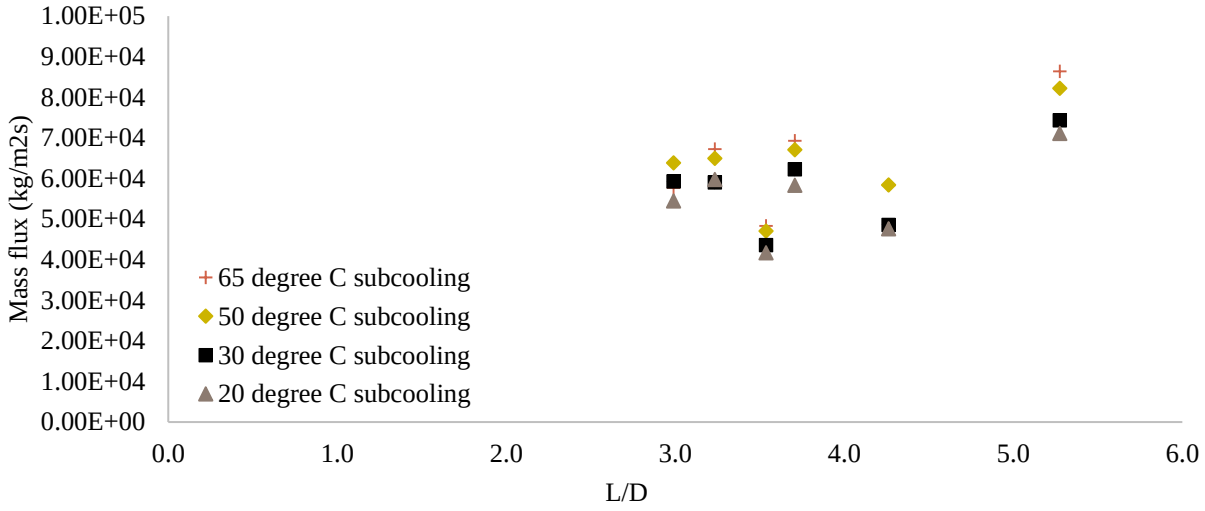

Figure 2-21 Mass flux versus L/D for the subcooled flashing tests at 4.14 MPa

2.6 Uncertainty of Mass Flux Experimental Data

The following procedure has been previously reported and discussed in Brown et. al [31].Error of the choking mass flux measurement is comprised of error of the crack's area measurement, linear expansion of the samples due to high water temperature, error of load cell calibration and error of averaging the results of load cell and differential pressure cell measurements.

The area of the cracks is measured by multiplying number of pixels inside the crack with the area of one pixel. A pixel is square; thus, its area is square of its side. The scale of 1mm used in the measurement has an error of 0.01mm. Counting the number of pixels in 1mm length has an error of 20 pixels due to the thickness of the marks on the scale. Length of a pixel is calculated as:

$$l = \frac{1}{N} \tag{2.3}$$

The error of (2.3), therefore, is:

$$\Delta l = \sqrt{\left(\frac{1}{N}\right)^2 * 0.01^2 + \frac{1}{N^4} * 20} = \frac{1}{N}\sqrt{0.01^2 + \frac{20}{N^2}} \tag{2.4}$$

As a result, area of a pixel and its error are calculated as:

$$a = l^2 => \Delta a = 2 * l * \Delta l \tag{2.5}$$

Assuming M an Z are number of pixels inside a crack and along perimeter of a crack respectively. Since along the perimeter, pixels can lie partly inside the crack, which makes an error of counting M. The error of M, therefore, is equal to 0.5*Z. Consequently, area of the crack and its error is:

$$A = M * a \tag{2.6}$$

$$\Delta A = \sqrt{a^2 * (\Delta M)^2 + M^2 * (\Delta a)^2} = \sqrt{a^2 * 0.25 * Z^2 + M^2 * 4 * l^2 * (\Delta l)^2} \tag{2.7}$$

The error of wetted perimeter, p, is calculated in the similar way ($\Delta Z = 1$):

$$p = Z * l => \Delta p = \sqrt{Z^2 * (\Delta l)^2 + l^2 * (\Delta Z)^2} = \sqrt{Z^2 * (\Delta l)^2 + l^2} \tag{2.8}$$

Length of a crack expands under high temperature. Linear expansion of the crack can be calculated as:

$$\int \frac{dL}{L} = \int \alpha dT \tag{2.9}$$

For 316SS, the mean coefficient of thermal expansion is 17.3 (μm/mK). Hence,

$$L = L_0 * \exp(\alpha \Delta T)$$

$$\Delta L = L_0 * (\exp(\alpha \Delta T) - 1) \tag{2.10}$$

Increase in crack's area due to thermal expansion:

$$\Delta A = b * \Delta L \tag{2.11}$$

The load cell has its error specified in the manual as 0.05% of the max reading scale (136.07kg). In addition, the load cell still has error coming from its calibration. In order to calibrate the load cell, we used a jug filled with water. The error comes from weighing the jug with water inside and this error is estimated to be 0.8g. The error is added into total error of load cell. The error of each load cell is calculated and equal to 0.0973kg.

There are two independent measurements for choking mass flux: load cell and differential pressure cell. Difference between the results of these two measurements constitutes the mass flux's measurement's error. The final result is calculated as a mean of load cell and differential pressure cell measurement. Therefore, standard error of the mean is determined as follow:

$$\Delta G_c = \frac{\left|G_{c,DP} - G_{c,LC}\right|}{2\sqrt{2}} \tag{2.12}$$

where $G_{c,DP}$ and $G_{c,LC}$ are choking mass flux measured by the differential pressure cell and the load cell respectively.

Relative error:

$$\frac{\Delta G_c}{G_c} = \frac{\frac{\left|G_{c,DP} - G_{c,LC}\right|}{2\sqrt{2}}}{\frac{G_{c,DP} + G_{c,LC}}{2}} = \frac{\left|G_{c,DP} - G_{c,LC}\right|}{\sqrt{2}\left(G_{c,DP} + G_{c,LC}\right)} \tag{2.13}$$

3. RELAP5 CHOKING FLOW MODEL ASSESSMENT

3.1 Choking Flow Models

3.1.1 Henry-Fauske Model

The default critical flow model for RELAP5/MOD3.3 is the Henry-Fauske (H-F) model. As previously discussed, the objective of this model is to predict choking using only stagnation conditions, while accounting for thermal non-equilibrium effects. The choking criterion given by Equation 3.3 is obtained by combining the one-dimensional momentum equation and mass flux for high velocities, Equations 3.1 and 3.2 [32].

$$-AdP = d\left(m_g u_g + m_f u_f\right) + dF \tag{3.1}$$

$$G = -\left\{\frac{d\left[xu_g + (1-x)u_f\right]}{dP}\right\}_t \tag{3.2}$$

$$G_c^2 = -\frac{1}{\left\{x\frac{\partial v_g}{\partial P} + (1-x)\frac{\partial v_f}{\partial P} + \left(v_g - v_f\right)\frac{\partial x}{\partial P}\right|\ \ \right\}_t} \tag{3.3}$$

Assuming polytropic process (n~1) the choking criterion simplifies to Equation 3.4.

$$G_c^2 = \left(\frac{1}{\frac{N}{G_{cHE}} - v_g x_{ex}\frac{dN}{dP}}\right)_{ex} \tag{3.4}$$

Again N is defined as the non-equilibrium parameter and can be calculated as follows,

$$N = \frac{v_l}{x_{ex}(1-\alpha)v_v} \tag{3.5}$$

3.1.2 Ransom Trapp Model

The choking criterion for the Ransom-Trapp (R-T) model is much more complex. It is designed to reflect physics that occur before and at the choking plane. This includes mixture continuity, two-phase momentum equations, mixture energy, and gas continuity. Ransom and Trapp account for non-equilibrium effects in the case of subcooled liquid at the choking plane. This effect is accounted for in RELAP5/MOD3.3 by applying the Alamgir and Lienhard correlation for pressure undershoot [33].

$$\Delta P = P_{sat} - P_t = \frac{0.258^{\sigma^{1.5}} T_R^{13.76}}{(k_B T_C)^{0.5}} \frac{v_g}{v_g - v_f} \left[1 + 2.078\, x\, 10^{-8} \left(\rho_f \frac{1}{A_t} \frac{dA_t}{d_x}\, u_c^3 \right)^{0.8} \right]^{\frac{1}{2}}$$
$$-6.9984\, x\, 10^{-2} \left(\frac{A_t}{A} \right)^2 \rho_f u_C^2 \tag{3.6}$$

The choked velocity can be calculated in the case of subcooled liquid flow by the expansion of the Bernoulli equation to the throat by

$$u_c = \sqrt{2\,(P_{up} - P_{sat})/\rho} \tag{3.7}$$

Due to applications to nozzle, orifices, and short tubes, flashing occurs at the choking plane, so two-phase choking criteria can also be employed where,

$$u_c = a \tag{3.8}$$

$$\pm\alpha_{HE} = \frac{\left(\alpha_g \rho_f u_g + \alpha_f \rho_g u_f\right)}{\alpha_g \rho_f + \alpha_f \rho_g} \tag{3.9}$$

3.1.3 RELAP5 Nodalization

The nodalization diagram used for this study can be seen in Figure 3-1.

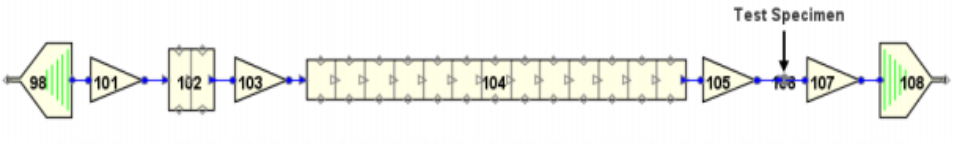

Figure 3-1 RELAP5 nodalization diagram

98 = P stagnation, time dependent

101 = Pipe junction

102 = Pipe (1 in. Dia., 2 in. long, 2 nodes)

103 = Abrupt area change pipe junction

104 = Sample length (13 or less nodes of 2.54 cm)

105 = ½ in pipe junction to crack

106 = Crack channel length, as a pipe, (5 or less nodes of 0.228 mm)

107 = "Choking Plane", pipe junction

108 = Back Pressure, time dependent

In all cases studied, the default model used for entrance losses in RELAP5/MOD3.3 is applied. RELAP5/MOD3.3 is used as a best estimate code and the fewer manual inputs used

determines the effectiveness of the code. Due to the smooth samples being studied, the wall roughness wasn't calculated as in previous simulated crack studies. This can calculation can be done by using the well known peak-to-valley method.

3.1.4 Simulation Results

The H-F and R-T models were both used to predict experimentally obtained values with the above mentioned nodalization. It is advised in the RELAP5/MOD3.3 manuals that a node size should be twice that of the hydraulic diameter [33]. This allows for 5 nodes along the channel length to be used in this analysis. Figure 3.2 shows the predictions of both the H-F and R-T models versus the experimental data of the current study. In general, the models strayed further away from the data as the stagnation pressure conditions and L/D ratios were increased. The H-F model over predicts the mass flux at high pressure and subcooling specifically for Sample 8. This alludes to thermal non-equilibrium breakdown of the model. The experimental data for Sample 10 shows a major discrepancy in mass flux by an order of magnitude. This can only be attributed due to an oversight in area calculation for this sample. Subsequently this data set is similar in L/D to that of Wolf and Vadlamani data sets and is compared within Figure 3-3. Figure 3-4 isolates the sample in question of this study. It is compared not only with those of similar area and hydraulic diameter but also stagnation pressure and subcooling conditions of Wolf's samples [34]

The R-T model drastically under predicts the data in most runs, and over prediction occurs at low pressure stagnation conditions. There isn't a clear separation between the predictions. In this case, neither model can be chosen as a superior choice in modeling such flow. If there was such a case which required the use of RELAP5/MOD3.3 to predict flows in very short channels, then a conservative point of view must be taken.

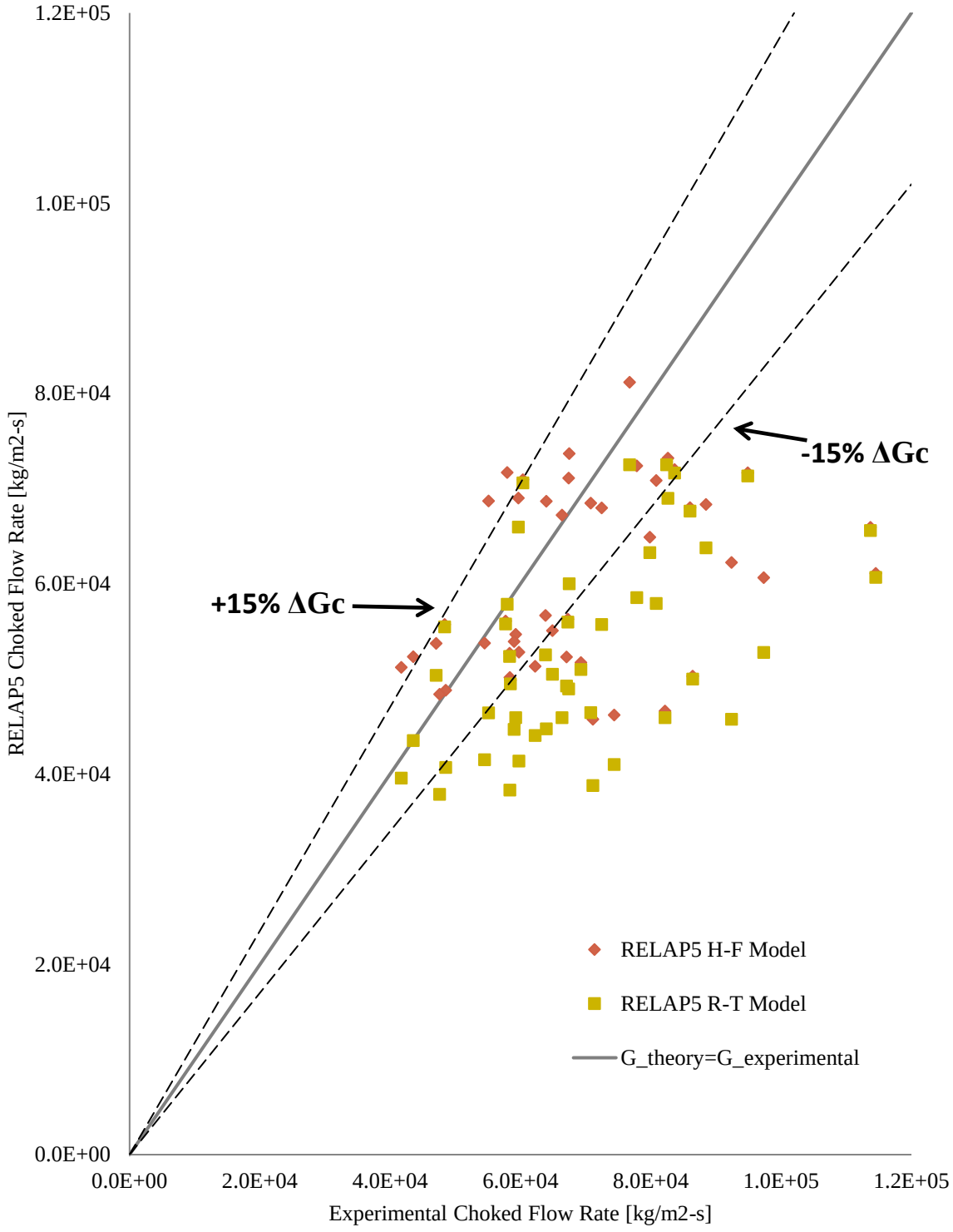

Figure 3-2 Comparison of H-F and R-T choked flow predictions to data of the current study

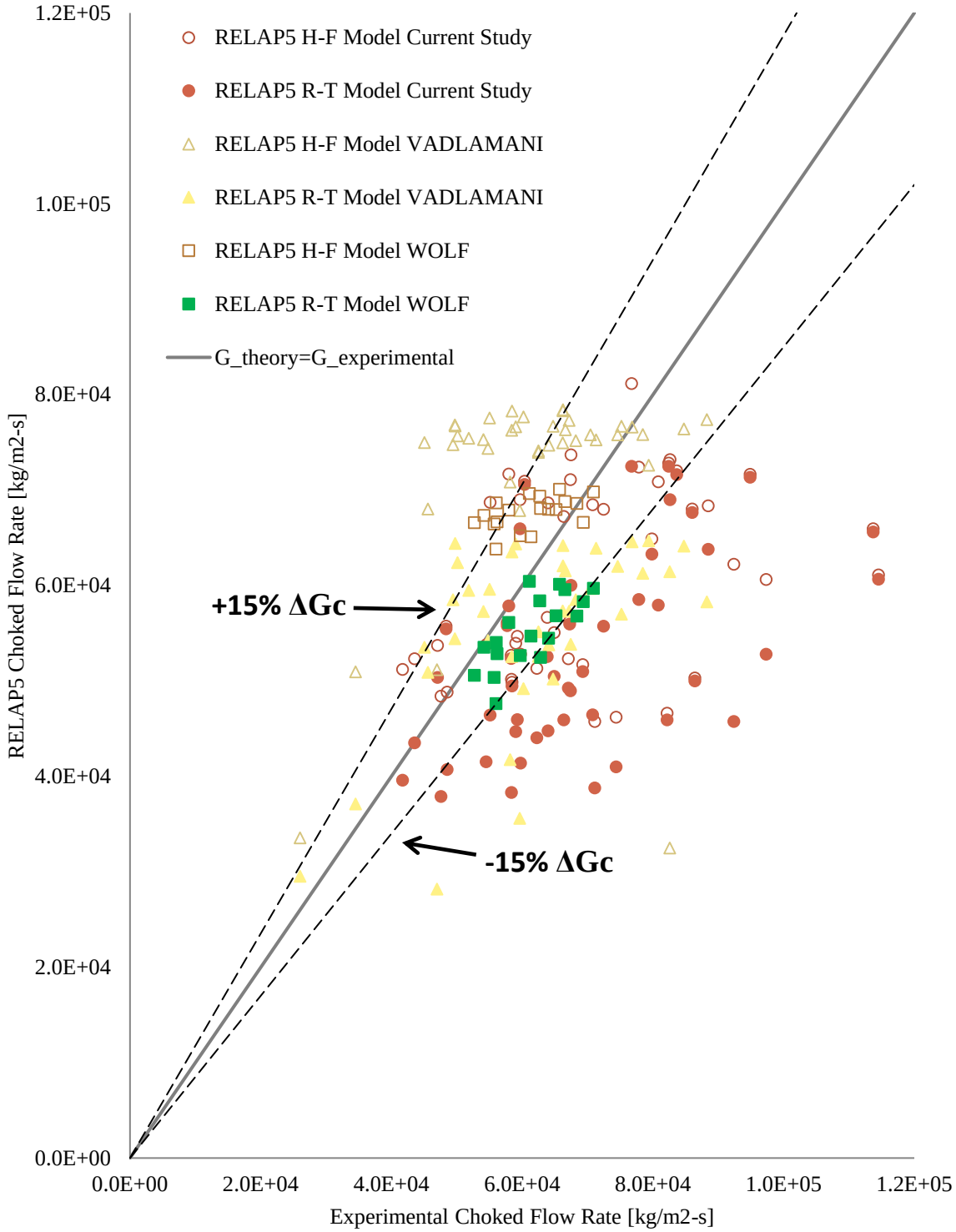

Figure 3-3 Comparison of HF and RT choked flow predictions to similar slits in literature

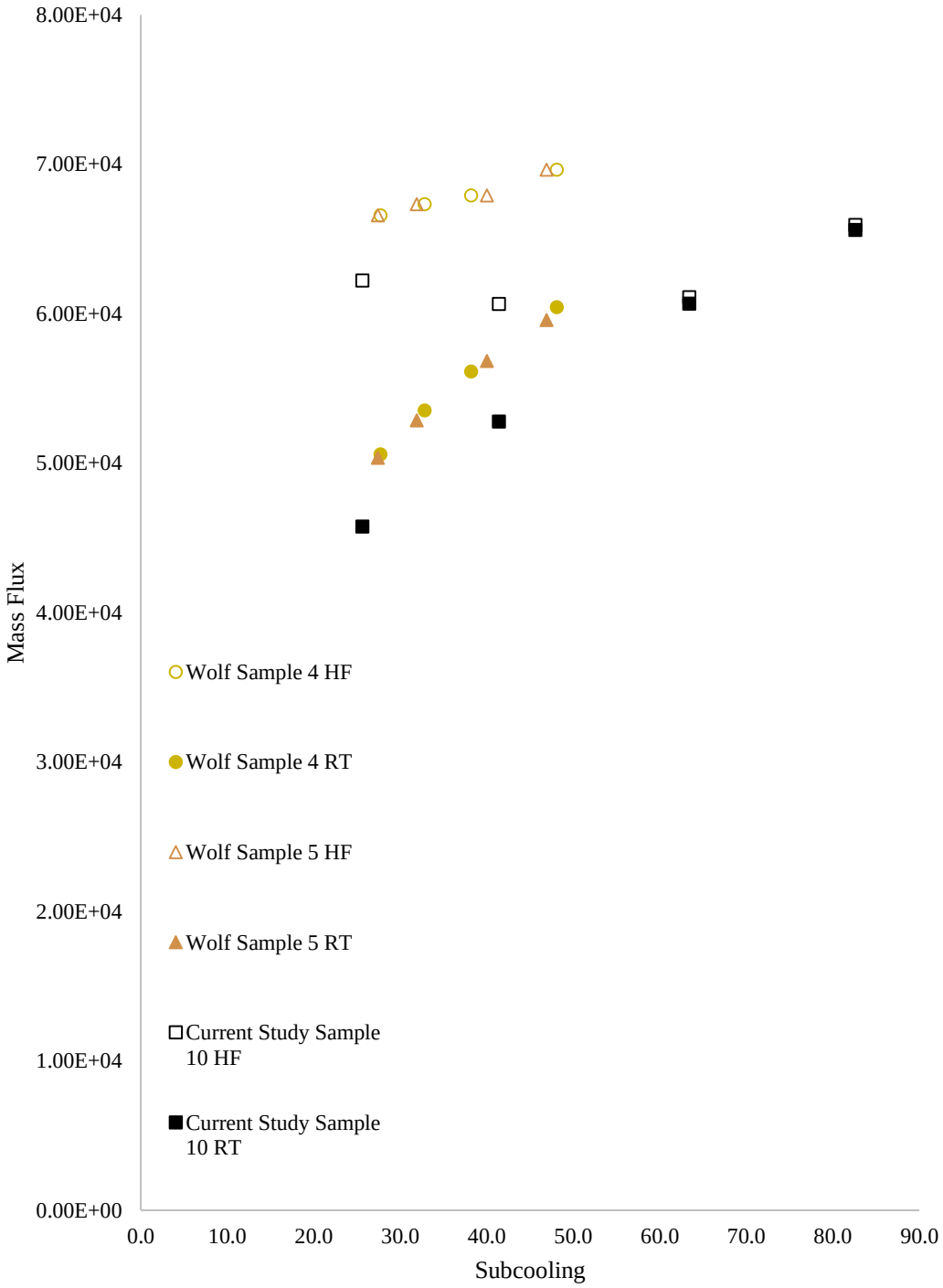

Figure 3-4 Isolated Sample Comparison to Similar Samples in Literature

4. SUMMARY AND CONCLUSIONS

Similar results have been reported and discussed in Brown et. al [31] for actual axial cracks of SG tube, whereas, a RELAP5/MOD3.3 nodalization was used to model and assess the prediction of experimental data from literature as well as the current experimental program data. It is found at high pressure stagnation conditions 6.89 MPa for channel length of 1.14 mm the H-F model overpredicts and the RT model under predicts for simulated cracks. The H-F and R-T model predictions begin to converge as the stagnation pressure decreases. In order to understand the difference for high pressure stagnation conditions, more investigation into the dependence of the throat pressure for each model needs to be done.

The experiment is designed to simulate pressure difference through SG tube wall, thus the most valuable data are at the highest pressure. It is difficult to assess the flow development along the channel length since the flow pressure profile cannot be measured experimentally. This is considered as a disadvantage when conducting this experiment on short channel lengths. While RELAP5/MOD3.3 has been shown to predict choking flow in large scale geometries, it is recommended not to depend on the predictions for small channel lengths discussed in this assessment. It's obvious for short channel lengths and low-pressure conditions these models start to converge. Prediction of the throat pressure by RELAP5/MOD3.3 may help determine why this occurs.

5. FUTURE WORK

The current study focused on simulated smooth SG tube cracks of channel length 1.14 mm. In order to further understand the friction component of actual SG tube cracks, a test matrix should be developed for samples with calculated surface roughness. There are techniques available through literature to correctly fabricate slit geometries with known surface roughness. Study of actual steam generator tube samples with cracks developed from industry degradation mechanism would be most beneficial. An adjustment to the testing facility to discharge at industry operating pressure conditions would be ideal. This would require stagnation conditions of 14 MPa and a back pressure of 6.89 MPa

Further insight of chemical shims present in the primary side may be considered as non-condensable gas will affect the choking phenomenon. As this is an ideal experiment, all runs were de-gassed. Overall, a model to capture the non-equilibrium effects over a short channel length needs further development.

REFERENCES

[1] R. E. Henry, “Two-Phase Critical Discharge of Initially Saturated or Subcooled Liquid,” *Nucl. Sci. Eng.*, vol. 41, no. 3, p. 336-, 1970.

[2] R. E. Henry and H. K. Fauske, “The Two-Phase Critical Flow of One-Component Mixtures in Nozzles, Orifices, and Short Tubes,” *J. Heat Transfer*, vol. 93, no. 2, p. 179, 1971.

[3] R. E. Henry, M. A. Grolmes, and H. K. Fauske, “Pressure Drop and Compressible Flow of Cryogenic Liquid-Vapor Mixtures,” in *Heat Transfer at Low Temperatures*, W. Frost, Ed. Boston, MA: Springer US, 1975, pp. 229–259.

[4] D. Abdollahian and B. Chexal, “Calculation of leak rates through cracks in pipes and tubes. Final report.”

[5] C. Amos and V. Schrock, “Critical Discharge of Initially Subcooled Water Through Slits,” *Nureg/Cr-3476*, 1983.

[6] H. John, J. Reimann, F. Westphal, and L. Friedel, “Critical Two-Phase Flow Through Rough Slits,” *Int. J. Multiph. Flow*, vol. 14, no. 2, pp. 155–174, 1988.

[7] R. P. Collier, F. B. Stuben, M. E. Mayfield, D. B. Pope, and P. M. Scott, “Two-phase flow through intergranular stress corrosion cracks,” *Electr. Power Res. Inst. Rep. EPRI-NP-3540-LD, Palo Alto, CA*, 1984.

[8] S. T. Revankar, B. Wolf, and J. R. Riznic, “Investigation of Subcooledwater Discharge Through Simulated Steam Generator Tube Cracks,” *Multiph. Sci. Technol.*, vol. 25, no. 2–4, pp. 249–285, 2013.

[9] S. G. Sadasiva, “Thesis / Dissertation Acceptance,” vol. 9, p. 2014, 2014.

[10] H. J. Yoon, M. Ishii, and S. T. Revankar, “Choking flow modeling with mechanical non-equilibrium for two-phase two-component flow,” *Nucl. Eng. Des.*, vol. 236, no. 18, pp. 1886–1901, 2006.

[11] H. Nguyen, M. Brown, S. T. Revankar, and J. Riznic, “Experimental Investigation of Subcooled Choking Flow in a Steam Generator Tube Crack,” in *Internatioanl Conference on Nuclear Engineering*, 2016, pp. 1–2.

[12] I. A. E. A. (IAEA-T.-1668) (IAEA), “Assessment and Management of Ageing of Major Nuclear Power Plant Components Important to Safety: Steam Generators.”

[13] E. Fuller, “Steam generator integrity assessment guidelines revision 2,” *Final Rep. Non-Proprietary Version EPRI*, vol. 1012987, no. July, 2006.

[14] K. C. Wade, “Steam Generator Degradation and Its Impact on Continued Operation of Pressurized Water Reactors in the United States by,” *Power*, no. August, 1995.

[15] O.C. Jones Jr., “Flashing Inception in Flowing Liquids,” *ASME J. Heat Transf.*, vol. 102, p. 439, 1980.

[16] J. Yang, O. C. Jones, and T. S. Shin, “Critical flow of initially subcooled flashing liquids: Limitations in the homogeneous equilibrium model,” *Nucl. Eng. Des.*, vol. 95, no. C, pp. 197–206, 1986.

[17] A. Agostinelli, V. Salemann, and N. J. Harrison, “Prediction of Flashing Water Flow Through Fine Annular Clearances,” *Am. Soc. Mech. Eng.*, vol. 80, pp. 1138–1142, 1958.

[18] R. J. Simoneau, “Two-Phase Choked Flow of Subcooled Nitrogen Through a Slit,” *Nasa*, 1974.

[19] S. T. Revankar, B. Wolf, and A. Vadlamani, *Subcooled Choked Flow through Steam Generator Tubes Final Report*. 2013.

[20] E. Elias and G. S. Lellouche, “Two-phase critical flow,” *Int. J. Multiph. Flow*, vol. 20, no. SUPPL. 1, pp. 91–168, 1994.

[21] E. S. Starkman, V. E. Schrock, and K. F. Neusen, “Expansion of a Very Low Quality Two-Phase Fluid Through a Convergent-Divergent Nozzle,” *Trans ASME, Basic Eng.*, vol. 86, no. 2, pp. 247–256, 1964.

[22] S. Levy, “Non-Equilibrium Flow Model Critical,” 1999.

[23] M. Alamgir and J. H. Lienhard, “Correlation of Pressure Undershoot During Hot-Water Depressurization,” *J. Heat Transfer*, vol. 103, 1981.

[24] H. K. Fauske, “Contribution to the Theory of Two-Phase, One-Component Critical Flow,” 1962.

[25] S. Levy, “Prediction of Two-Phase Critical Flow Rate,” *J. Heat Transfer*, vol. 87, pp. 53–58, 1965.

[26] F. J. Moody, “Maximum Flow Rate of a Single Component Two-Phase Mixture,” *J. Heat Transfer*, vol. 87, pp. 134–142, 1965.

[27] G. B. Wallis, “Critical two-phase flow,” *Int. J. Multiph. Flow*, vol. 6, no. 1–2, pp. 97–112, 1980.

[28] M. Ishii, “One-Dimensional Drift-Flux Model and Constitutive Equations for Relative Motion Between Phases in Various Two-Phase Flow Regimes, ANL-77-47,” 1977.

[29] M. Ishii and T. Hibiki, *Thermo-Fluid Dynamics of Two-Phase Flow*. 2011.

[30] S. T. Revankar, B. Wolf, and J. R. Riznic, “Flashing flow of subcooled liquid through small cracks,” *Procedia Eng.*, vol. 56, pp. 454–461, 2013.

[31] M. A. Brown, H. Nguyen, S. T. Revankar, and J. Riznic, “Assessment of Choking Flow Models in RELAP5 for Subcooled Choking Flow Through a Small Axial Crack of a Steam Generator Tube,” in *Internatioanl Conference on Nuclear Engineering*, 2017, pp. 6–8.

[32] L. Sokolowski, T. Kozlowski, and A. Calvo, “Assessment of Two-Phase Critical Flow Models Performance in RELAP5 and TRACE Against Marviken Critical Flow Tests,” *Trans. Am. Nucl. Soc.*, vol. 102, no. February, p. 85, 2012.

[33] K. Carlson, R. Riemke, and S. Rouhani, “RELAP5/MOD3 code manual, Volume IV: Models and Correlations (Draft),” *Idaho Natl. Eng. ...*, vol. IV, 1990.

[34] B. J. Wolf, “Subcooled Choked Flow Through Steam Generator Tube Cracks,” Purdue University, 2012.